

Simulating electronic structure on bosonic quantum computers

Rishab Dutta,[†] Nam P. Vu,[‡] Ningyi Lyu,[†] Chen Wang,[¶] and Victor S. Batista^{†,§}

[†]*Department of Chemistry, Yale University, New Haven, CT 06520, USA*

[‡]*Department of Chemistry, Lafayette College, Easton, PA 18042, USA*

[¶]*Department of Physics, University of Massachusetts-Amherst, Amherst, MA 01003, USA*

[§]*Yale Quantum Institute, Yale University, New Haven, CT 06511, USA*

Abstract

Computations with quantum harmonic oscillators or qumodes is a promising and rapidly evolving approach towards quantum computing. In contrast to qubits, which are two-level quantum systems, bosonic qumodes can in principle have infinite discrete levels, and can also be represented with continuous variable bases. One of the most promising applications of quantum computing is simulating many-fermion problems such as molecular electronic structure. Although there has been a lot of recent progress on simulating many-fermion systems on qubit-based quantum hardware, they can not be easily extended to bosonic quantum devices due to the fundamental difference in physics represented by qubits and qumodes. In this work, we show how an electronic structure Hamiltonian can be transformed into a system of qumodes with a fermion to boson mapping scheme and apply it to simulate the electronic structure of dihydrogen molecule as a system of two qumodes. Our work opens the door for simulating many-fermion systems by harnessing the power of bosonic quantum devices.

1 Introduction

Understanding the ground and excited states of many-fermion systems is one of the fundamental problems in chemistry and physics. Accurate simulation of molecular electronic structure, a many-fermion problem, is critical in understanding chemical reaction mechanisms or designing new molecules and materials with novel properties. Classical computers are fundamentally restricted in simulating molecular electronic structure problems beyond a certain system size,¹ and the recent interest in developing algorithms based on quantum computers can potentially address this issue.

The current era of noisy intermediate scale quantum (NISQ) computers relies on the quantum information unit known as qubits which are two-level quantum systems. NISQ computers have inherent limitations due to the decoherence associated with qubits and the quantum operators acting on them. Nevertheless, several hybrid quantum-classical algorithms have been developed to simulate molecular electronic structure, that combines resources from both classical and quantum devices.²⁻⁷ One of the steps in all these algorithms involves mapping the fermionic Hamiltonian of the molecule of interest to a qubit Hamiltonian.^{8,9}

The development of bosonic quantum devices introduces a fundamentally novel approach to quantum computing. Bosonic quantum computing can be conceptually understood as computations with quantum harmonic oscillators (QHOs), also known as *qumodes*, instead of qubits. Qumodes can store quantum information in the unbounded Hilbert space of QHOs and naturally support continuous variable bases due to the position and momentum operators associated with oscillator modes. A range of applications have been demonstrated using bosonic quantum devices for chemistry,¹⁰ including simulation of molecular vibronic spectra,^{11,12} understanding conical intersections,¹³ and implementing quantum dynamics for modeling chemical processes.¹⁴

Qumodes can be realized with different hardware approaches,¹⁵ including but not limited to electromagnetic fields inside resonators,^{16,17} the motions of trapped ions,¹⁸ or a network of

optical devices,¹¹ as shown in Figure 1. A promising and rapidly evolving hardware platform for realizing bosonic quantum computation is the circuit quantum electrodynamics (cQED) approach.^{19,20} The cQED hardware comprises of microwave resonators as the qumodes, and superconducting circuits based on Josephson junctions act as the non-linear element that controls and measures the quantum information. Bosonic cQED devices with 3D resonator geometries can have a lifetime of up to milliseconds, and provide a robust platform for understanding decoherence from photon loss.¹⁵

Quantum algorithms for molecular electronic structure tailored for qubits can not be trivially applied to qumode hardware due to the fundamental difference between qubits which are spin-1/2 systems and qumodes which are bosonic. An important step in simulating molecular electronic structure on bosonic quantum computers would be to map the corresponding fermionic Hamiltonian to a bosonic one. There has been substantial past work on fermion to boson mapping, including exact and approximate transformations.^{21–28} However, these transformations lack a direct exact operator mapping between fermions and bosons beyond the case where the fermions are paired. We focus on two fermion to boson transformations here that have largely been overlooked by the electronic structure community. An exact state mapping between fermionic Slater determinants and bosonic Fock states of QHOs was established by Ohta based on the fact that particle-hole excitations from the Fermi vacuum can be represented as photon transitions.²⁹ An exact operator mapping between a number-conserving bilinear fermionic operator and oscillator projection operators can be derived from this state mapping, as shown by Dhar, Mandal, and Suryanarayana.³⁰

In this work, we apply fermion to boson mapping for transforming the molecular electronic structure Hamiltonian to a system of qumodes and apply it to the dihydrogen molecule. To the best of our knowledge, this is the first time a molecular electronic structure Hamiltonian has been simulated as a bosonic system. We also introduce a hybrid quantum-classical approach for finding the ground state energy of a molecule, where the computation of the expectation value of the mapped bosonic Hamiltonian may be done on a bosonic quantum

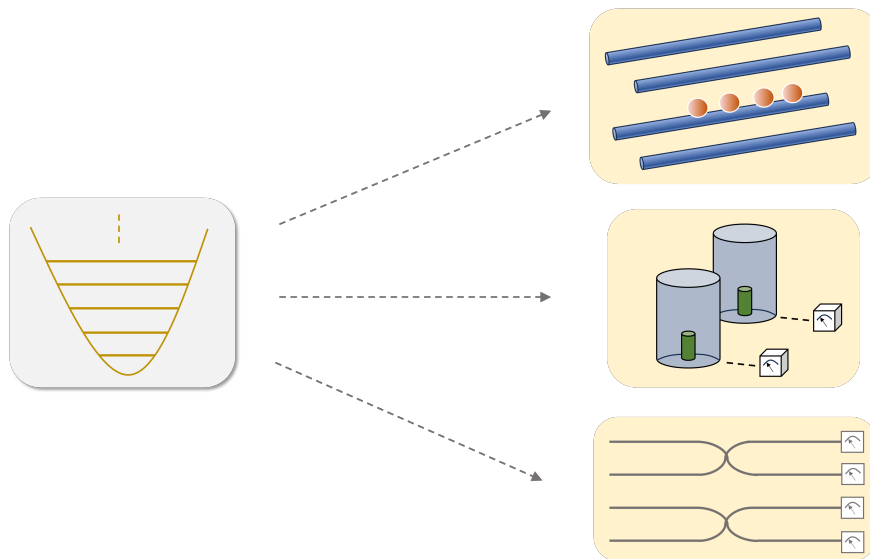


Figure 1: A quantum harmonic oscillator or qumode offers a new way to approach quantum computing beyond qubits. Different hardware options are possible to build qumodes. The top schematic on the right represents an ion trap where collective vibrations of the ions act as the qumodes. The orange spheres are the ions and the blue rods are a set of electrodes. The schematic on the middle of right represents the cavity quantum electrodynamics approach where superconducting resonators act as qumodes. The grey cylinders are microwave resonators and they are connected to the superconducting circuit via the green center pins. The bottom schematic on the right represents the photonic approach where the photonic modes act as qumodes.

computer with the trial energy optimized on a classical computer. Although this work focuses specifically on the molecular electronic structure Hamiltonian, the techniques presented here can be applied to any number-conserving many-fermion Hamiltonian such as systems studied in condensed matter³¹ or nuclear physics.²¹

2 Background

We will motivate the electronic structure problem, before discussing some key concepts related to representing electrons algebraically here.

2.1 Motivation

The molecular Hamiltonian in atomic units can be written as³²

$$\mathcal{H} = -\frac{1}{2} \sum_i \nabla_i^2 - \frac{1}{2} \sum_A \frac{\nabla_A^2}{M_A} - \sum_i \sum_A \frac{Z_A}{r_{iA}} + \sum_i \sum_{j>i} \frac{1}{r_{ij}} + \sum_A \sum_{B>A} \frac{Z_A Z_B}{R_{AB}}, \quad (1)$$

where i, j are electron indices, A, B are nuclear indices, ∇_i^2 and ∇_A^2 are Laplacian operators representing differentiation with respect to the coordinates of the i^{th} electron and A^{th} nucleus, M_A and Z_A are the mass and atomic number of nucleus A , $r_{iA} = |\mathbf{r}_i - \mathbf{R}_A|$ is the distance between i^{th} electron and A^{th} nucleus, $r_{ij} = |\mathbf{r}_i - \mathbf{r}_j|$ is the distance between i^{th} and j^{th} electrons, and $R_{AB} = |\mathbf{R}_A - \mathbf{R}_B|$ is the distance between A^{th} and B^{th} nuclei. The operator terms in Eq. (1) represent the kinetic energy of electrons, kinetic energy of nuclei, Coulomb attraction between electrons and nuclei, repulsion between electrons, and repulsion between nuclei, respectively.

The Born–Oppenheimer approximation assumes the molecular electrons are moving in the field of fixed nuclei since they are much lighter.³² This allows one to neglect the nuclear kinetic energy term in Eq. (1) and consider the nuclear-nuclear repulsion term to be constant. Thus, the remaining terms of Eq. (1) constitute the molecular electronic structure Hamiltonian

$$\mathcal{H}_{\text{elec}} = -\frac{1}{2} \sum_i \nabla_i^2 - \sum_i \sum_A \frac{Z_A}{r_{iA}} + \sum_i \sum_{j>i} \frac{1}{r_{ij}}. \quad (2)$$

Our goal is to solve the time-independent Schrödinger equation for the molecular electronic structure

$$\mathcal{H}_{\text{elec}} \Psi_\mu(\mathbf{r}) = E_\mu \Psi_\mu(\mathbf{r}) \quad (3)$$

where $\{\Psi_\mu\}$ are the electronic wavefunctions with corresponding energies $\{E_\mu\}$ for a given molecular nuclear coordinates. As an example, Ψ_0 and E_0 are the ground electronic wavefunction and its energy. Finding the $\{\Psi_n\}$ wavefunctions on a classical computer is a notoriously hard problem because of the combinatorial growth of the dimensionality with increasing

number of electrons N in the molecule. This is where quantum computing promises to be impactful.

2.2 Second quantization

An electronic wavefunction $\Psi(\mathbf{r})$ depends on a set of N electron coordinates $\{\mathbf{r}_j\}$. However, one should also include the electron spin into the picture, and denote the wavefunction as $\Psi(\mathbf{x})$ instead, where \mathbf{x} represents the combined spatial and spin coordinates of the electrons. Spin does not fundamentally arise in the non-relativistic premise of electronic structure theory. Nevertheless, spin must be included as a bookkeeping tool to respect the fermionic antisymmetry of electrons

$$\Psi(\cdots, \mathbf{x}_j, \cdots, \mathbf{x}_k, \cdots) = -\Psi(\cdots, \mathbf{x}_k, \cdots, \mathbf{x}_j, \cdots), \quad (4)$$

even in approximate wavefunctions. A good starting point for approximately solving the electronic structure is the Hartree–Fock (HF) method,³² which transform the many-electron problem of Eq. (3) to an effective one-electron problem in the mean-field created by the other electrons. The HF method provides M number ($M > N$) of orthonormal one-electron functions $\{\chi_p(\mathbf{x})\}$, called the molecular spin-orbitals. We are assuming M to be an even integer since there is an underlying $M/2$ number of spatial functions $\{\phi_p(\mathbf{r})\}$ which can associate with either up-spin $\alpha(\omega)$ or down-spin $\beta(\omega)$ functions

$$\chi_{2p-1}(\mathbf{x}) \equiv \phi_p(\mathbf{r}) \alpha(\omega), \quad \chi_{2p} \equiv \phi_p(\mathbf{x}) \beta(\omega). \quad (5)$$

Thus, N electrons in M molecular spin-orbitals give rise to $\binom{M}{N}$ number of many-electron basis states, each of which is an antisymmetrized product state

$$|p_1, \dots, p_N\rangle_F \equiv \frac{1}{\sqrt{N!}} \begin{vmatrix} \chi_{p_1}(\mathbf{x}_1) & \cdots & \chi_{p_N}(\mathbf{x}_1) \\ \chi_{p_1}(\mathbf{x}_2) & \cdots & \chi_{p_N}(\mathbf{x}_2) \\ \dots & \ddots & \dots \\ \chi_{p_1}(\mathbf{x}_N) & \cdots & \chi_{p_N}(\mathbf{x}_N) \end{vmatrix}, \quad (6)$$

where $0 \leq p_1 < \dots < p_N \leq M - 1$. The wavefunction in Eq. (6) is the so-called Slater determinant and based on the ordering of $\{p_j\}$ indices, approximates the exact ground and excited electronic states. For example, the Slater determinant $|0, \dots, N - 1\rangle_F$ is the electronic ground state wavefunction under the HF approximation.

One point to notice in Eq. (6) is that any Slater determinant can be uniquely identified by asking which spin-orbitals are occupied for a given set of spin-orbitals. This leads to the second quantization formulation in terms of fermionic creation operators $\{f_p^\dagger\}$ and annihilation operators $\{f_p\}$. These elementary fermionic operators follow the canonical anticommutation relation (CAR)

$$\{f_p^\dagger, f_q^\dagger\} = f_p^\dagger f_q^\dagger + f_q^\dagger f_p^\dagger = 0, \quad (7a)$$

$$\{f_p, f_q^\dagger\} = f_p f_q^\dagger + f_q^\dagger f_p = \delta_{pq}, \quad (7b)$$

where the fermionic mode indices represent the M number of spin-orbital functions $\{\chi_p\}$. The Pauli exclusion principle is then equivalent to the relation $(f_p^\dagger)^2 = 0$, which is simply a consequence of the CAR in Eq. (7). Thus, a given spin-orbital is either occupied or unoccupied. The Slater determinants are now defined as

$$|p_1, \dots, p_N\rangle_F \equiv f_{p_1}^\dagger \cdots f_{p_N}^\dagger |-\rangle_F, \quad (8)$$

where $|- \rangle_F$ is the physical vacuum representing the state with $N = 0$ electrons and any $f_p |- \rangle_F = 0$.

The electronic Hamiltonian can be represented in the molecular spin-orbital basis as³³

$$H_{\text{elec}} = \sum_{pq} h_q^p f_p^\dagger f_q + \frac{1}{2} \sum_{pqrs} v_{rs}^{pq} f_p^\dagger f_q^\dagger f_r f_s, \quad (9)$$

where p, q, r, s indices represent the spin-orbitals and the scalars $\{h_q^p\}$ and $\{v_{rs}^{pq}\}$ are the one-electron and the two-electron integrals

$$h_q^p = \int d\mathbf{x} \chi_p^*(\mathbf{x}) \left(-\frac{1}{2} \nabla^2 - \sum_A \frac{Z_A}{r_A} \right) \chi_q(\mathbf{x}), \quad (10a)$$

$$v_{rs}^{pq} = \int d\mathbf{x}_1 d\mathbf{x}_2 \frac{\chi_p^*(\mathbf{x}_1) \chi_q^*(\mathbf{x}_2) \chi_r(\mathbf{x}_2) \chi_s(\mathbf{x}_1)}{r_{12}}, \quad (10b)$$

which is a byproduct of running a HF calculation. We will assume real-valued molecular orbitals from now on which leads to the following relations between electron integral tensor elements

$$h_q^p = h_p^q, \quad (11a)$$

$$v_{rs}^{pq} = v_{qs}^{pr} = v_{rp}^{sq} = v_{qp}^{sr}, \quad (11b)$$

in addition to $v_{rs}^{pq} = v_{sr}^{qp}$ due to the indistinguishability of electrons. It is then possible to write H_{elec} in a more compact form

$$\begin{aligned} H_{\text{elec}} = & \left[\frac{1}{2} \sum_p h_p^p f_p^\dagger f_p + \sum_{p>q} \left(h_q^p f_p^\dagger f_q + \frac{1}{2} \tau_{pq}^{pq} f_p^\dagger f_q^\dagger f_p f_q \right) \right. \\ & + \sum_{p>q>r} \left(\tau_{pr}^{pq} f_p^\dagger f_q^\dagger f_p f_r + \tau_{qr}^{pq} f_p^\dagger f_q^\dagger f_q f_r + \tau_{qr}^{pr} f_p^\dagger f_r^\dagger f_q f_r \right) \\ & \left. + \sum_{p>q>r>s} \left(\tau_{rs}^{pq} f_p^\dagger f_q^\dagger f_r f_s + \tau_{qs}^{pr} f_p^\dagger f_r^\dagger f_q f_s + \tau_{qr}^{ps} f_p^\dagger f_s^\dagger f_q f_r \right) \right] + \text{h.c.}, \quad (12) \end{aligned}$$

where we have defined $\tau_{rs}^{pq} \equiv v_{rs}^{pq} - v_{sr}^{pq}$ such that

$$\tau_{rs}^{pq} = \tau_{rs}^{qp} = -\tau_{sr}^{pq} = \tau_{pq}^{rs}, \quad (13)$$

and h.c. represents the Hermitian conjugate of its preceding operator term.

Each term of the electronic Hamiltonian in Eq. (12) has creation and annihilation operators in pairs, which reflects the fact that H_{elec} is number-conserving. We now define the bilinear fermionic operators³⁴

$$E_q^p \equiv f_p^\dagger f_q = (E_p^q)^\dagger, \quad (14)$$

which is equivalent to the number operator when $p = q$ and generalized singles excitation otherwise.³⁵ A set of $\{E_q^p\}$ can be successively applied to transform between any two Slater determinants with the same number of electrons. The bilinear fermionic operators follow a simple commutation relation

$$[E_q^p, E_s^r] = \delta_{qr} E_s^p - \delta_{ps} E_q^r, \quad (15)$$

and generate the $u(M)$ Lie algebra.³⁶ Thus, we can rewrite the electronic Hamiltonian as

$$\begin{aligned} H_{\text{elec}} = & \left[\frac{1}{2} \sum_p h_p^p E_p^p + \sum_{p>q} \left(h_q^p E_q^p + \frac{1}{2} \tau_{qp}^{pq} E_p^p E_q^q \right) \right. \\ & + \sum_{p>q>r} \left(\tau_{rp}^{pq} E_p^p E_r^q + \tau_{qr}^{pq} E_q^q E_r^p + \tau_{rq}^{pr} E_r^r E_q^p \right) \\ & \left. + \sum_{p>q>r>s} \left(\tau_{sr}^{pq} E_r^p E_s^q + \tau_{sq}^{pr} E_q^p E_s^r + \tau_{rq}^{ps} E_q^p (E_s^r)^\dagger \right) \right] + \text{h.c.}, \quad (16) \end{aligned}$$

where we have applied the adjoint relation for the bilinear fermionic operators and the relations in Eq. (13). Thus, we have written Eq. (16) in such a way that the knowledge about the bilinear fermionic operators $\{E_q^p\}$ with $p \geq q$ is sufficient to represent H_{elec} .

3 Fermion to boson mapping

Our goal is to map Eq. (8) to a bosonic state and Eq. (9) to a bosonic Hamiltonian, so that the molecular electronic structure problem can be tackled with bosonic quantum computers. The key results that we apply in this work are given below.

- A system with N fermions can be mapped to a system of N quantum harmonic oscillators (QHOs) or bosonic modes with a maximum of $M - N + 1$ oscillator levels for each.
- An exact injective state mapping exists between Slater determinants and Fock states of QHOs.
- An exact mapping exists between $\{E_q^p\}$ and Fock state projection operators of QHOs.

We mention the details below.

3.1 State mapping

Elementary bosonic operators follow the canonical commutation relation (CCR)

$$[b_p^\dagger, b_q^\dagger] = b_p^\dagger b_q^\dagger - b_q^\dagger b_p^\dagger = 0, \quad (17a)$$

$$[b_p, b_q^\dagger] = b_p b_q^\dagger - b_q^\dagger b_p = \delta_{pq}, \quad (17b)$$

where b_p^\dagger and b_p are the bosonic creation and annihilation operators. These operators are defined such that their action on the Fock state $\{|q\rangle \mid 0 \leq q \leq \infty\}$ of a single qumode is

$$b^\dagger |q\rangle_B \equiv \sqrt{q+1} |q+1\rangle_B, \quad (18a)$$

$$b |q\rangle_B \equiv \sqrt{q} |q-1\rangle_B, \quad q > 0 \quad (18b)$$

$$b |0\rangle_B \equiv 0, \quad (18c)$$

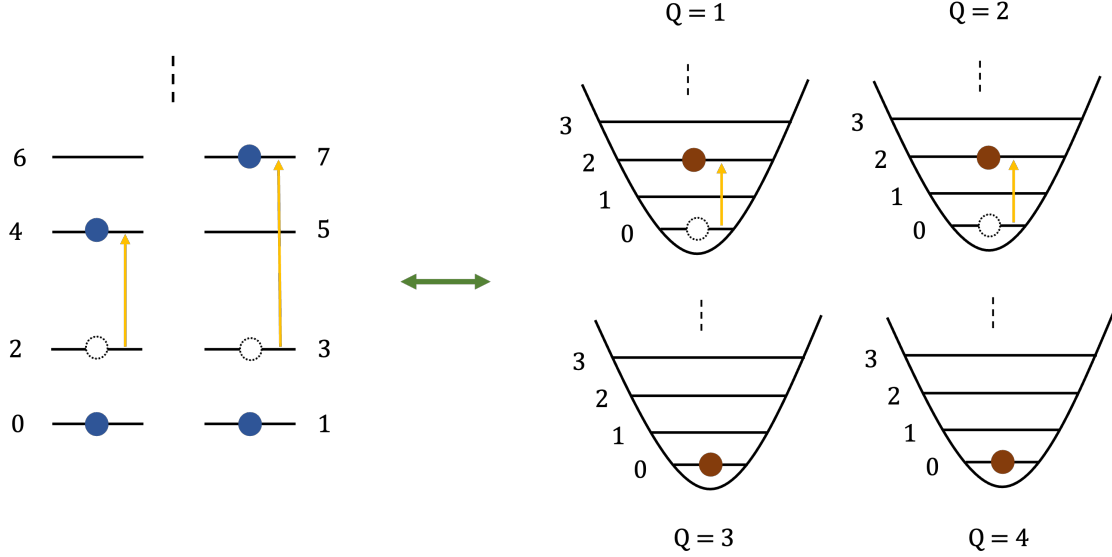


Figure 2: State diagrams corresponding to the state mapping as defined in Eq. (20) and Eq. (21). Here, a system with $N = 4$ electrons is mapped to a system of four quantum harmonic oscillators. In the initial state, the Slater determinant $|0, 1, 2, 3\rangle_F$ corresponds to four electrons occupying the lowest four spin-orbitals, which is mapped to the oscillator vacuum state $|0, 0, 0, 0\rangle_B$. When some of the occupied spin-orbitals are now excited to get the Slater determinant $|0, 1, 4, 7\rangle_F$, it gets mapped to the Fock state $|2, 2, 0, 0\rangle_B$. The occupied spin-orbitals for electrons and excitation levels for oscillators are represented by blue and brown circles, respectively.

which can be trivially generalized to multimodal bosonic systems by taking tensor products of single-mode Fock states. Similar to the fermionic case, the bosonic mode indices in Eq. (17) represent an orthogonal one-particle basis. Each of the bosonic or QHO mode can have infinite levels or occupancies since there is no nilpotency in the CCR. Thus, we define a Fock state of N QHOs as

$$|q_1, \dots, q_N\rangle_B \equiv \frac{(b_1^\dagger)^{q_1} \dots (b_N^\dagger)^{q_N}}{\sqrt{q_1! \dots q_N!}} |0, \dots, 0\rangle_B, \quad (19)$$

where $|0, \dots, 0\rangle_B$ is the ground state of the N oscillators. It should be noted that we only require a bosonic Fock basis of Eq. (19) for this paper, and our approach is agnostic of the properties of the underlying oscillators such as their anharmonicity.

The indices in Eq. (19) represent occupied levels of each mode, in contrast to Eq. (8) where

the occupied modes themselves are indexed. This distinction between Eq. (8) and Eq. (19) is simply the result of Pauli exclusion principle and how we have chosen the index ordering in Eq. (8). For example, the bosonic states $|2, 2\rangle_B$, $|2, 3\rangle_B$, $|3, 2\rangle_B$, and $|3, 3\rangle_B$ are all legitimate bosonic states involving the second and third levels of two bosonic modes, whereas $|2, 3\rangle_F$ is the only legitimate fermionic state involving the second and third spin-orbitals. Note that $|2, 3\rangle_F = f_2^\dagger f_3^\dagger |-\rangle_F = -f_3^\dagger f_2^\dagger |-\rangle_F$ respects the permutation of its underlying operators and the resulting sign change, which is similarly true for any Slater determinant defined in Eq. (8).

An injective state mapping exists between Slater determinants of N fermions defined in Eq. (8) and state of N QHOs defined in Eq. (19)^{29,37}

$$|p_1, \dots, p_N\rangle_F \leftrightarrow |q_1, \dots, q_N\rangle_B, \quad (20)$$

where the relation between the two sets of indices are

$$q_j = p_1, \quad \text{if } j = N, \quad (21a)$$

$$= p_{N-j+1} - p_{N-j} - 1, \quad \text{otherwise.} \quad (21b)$$

We refer the reader to Appendix A for a justification of the state mapping. Clearly, the Fermi vacuum $|0, \dots, N-1\rangle_F$ maps to the Fock ground state $|0, \dots, 0\rangle_B$ following Eq. (21). Then the physical interpretation of Eq. (20) is that the holes created from the Fermi vacuum and their impact on it are regarded as bosonic excitations, as in photoelectron spectroscopy. A schematic for an example state mapping of a system with $N = 4$ electrons is shown in Figure 2.

It is thus possible to apply the state mapping of Eq. (20) to map the full configuration

interaction (FCI) state for an N -fermion system as

$$|\Psi\rangle = \sum_{1 \leq p_1 < \dots < p_N \leq M} C_{p_1 \dots p_N} |p_1, \dots, p_N\rangle_F \mapsto \sum_{1 \leq q_1 < \dots < q_N \leq M} C_{p_1 \dots p_N} |q_1, \dots, q_N\rangle_B, \quad (22)$$

where the scalars $\{C_{p_1 \dots p_N}\}$ are the FCI coefficients and the $\{q_j\}$ indices are defined in Eq. (21). Since any N -fermion state can be represented as a special case of FCI, Eq. (22) allows mapping any state corresponding to a fermionic system with a fixed particle number to a bosonic state with the number of modes same as the number of fermions. Based on Eq. (21), it is easy to see that the highest integer corresponding to the indices $\{q_j\}$ in Eq. (22) is $L = M - N$. Thus, the state mapping naturally truncates the dimension of the Fock basis, i.e., number of qumode levels, based on the M number of spin-orbitals for a given electronic system, which makes the relevant bosonic Hilbert space isomorphic to the Hilbert space of N qudits³⁸ of $M - N + 1$ dimension.

As a specific example, let us discuss the state mapping of Eq. (20) for a system with $N = 2$ with arbitrary $M > 2$ number of spin-orbitals. Mapping between an arbitrary Slater determinant

$$|p, q\rangle_F \equiv f_p^\dagger f_q^\dagger |-\rangle_F, \quad (23)$$

and the mapped state of two qumodes

$$|j, k\rangle_B \equiv \frac{1}{\sqrt{j! k!}} (b_1^\dagger)^j (b_2^\dagger)^k |0, 0\rangle_B \quad (24)$$

is given by the following relations

$$p = k, \quad j = q - p - 1, \quad q = j + k + 1. \quad (25)$$

For example, if $M = 4$, then the transformations are

$$|0, 1\rangle_F \leftrightarrow |0, 0\rangle_B, \quad |0, 2\rangle_F \leftrightarrow |1, 0\rangle_B, \quad |0, 3\rangle_F \leftrightarrow |2, 0\rangle_B, \quad (26a)$$

$$|1, 2\rangle_F \leftrightarrow |0, 1\rangle_B, \quad |1, 3\rangle_F \leftrightarrow |1, 1\rangle_B, \quad |2, 3\rangle_F \leftrightarrow |0, 2\rangle_B. \quad (26b)$$

We have so far focused on mapping a Slater determinant into a multimodal bosonic state, but as evident from Eq. (20), the reverse is also true. For example, we write the bosonic states that did not appear in Eq. (26) but still correspond to two harmonic oscillator modes with three levels below

$$|1, 2\rangle_B \leftrightarrow |2, 4\rangle_F, \quad |2, 1\rangle_B \leftrightarrow |1, 4\rangle_F, \quad |2, 2\rangle_B \leftrightarrow |2, 5\rangle_F, \quad (27)$$

which are mapped to a Slater determinants of a $N = 2$ system that have $M > 4$ spin-orbitals.

3.2 Operator mapping

The Dhar–Mandal–Suryanarayana (DMS) transformation maps $\{E_q^p\}$ operators into Fock state projection operators of QHOs.³⁰ The DMS transformation was derived from the state mapping of Eq. (20) in Ref. 30. We simply state the resulting expressions of the DMS transformation here and refer the reader to Appendix B for more insight into its derivation.

Let us define the bosonic Fock space projection operator corresponding to a given set of k harmonic oscillator modes as

$$\mathcal{P}_{r_1, \dots, r_k} \equiv |r_1, \dots, r_k\rangle \langle r_1, \dots, r_k|, \quad (28)$$

and similarly define a related operator as

$$\mathcal{C}_{k,a} = \sum_{\substack{r_1 + \dots + r_k \\ = a}} \mathcal{P}_{r_1, \dots, r_k}, \quad (29)$$

where each index $\{r_j \mid 0 \leq r_j \leq L\}$ has a specific range based on the highest physical mode level that needs to be accessed following the state mapping. The expectation value of the operator in Eq. (29) can be computed from the same set of photon number measurements. Let us also denote the identity operator acting on the first k harmonic oscillator modes as

$$\mathcal{I}_k \equiv \mathbb{I}_1 \otimes \cdots \otimes \mathbb{I}_k. \quad (30)$$

Then the DMS mapping for any number operator E_p^p is

$$E_p^p \mapsto \mathcal{I}_{N-1} \otimes |p\rangle \langle p| + \sum_{k=1}^{N-1} \mathcal{I}_{k-1} \otimes \mathcal{C}_{N-k+1, p-N+k}, \quad (31)$$

where $0 \leq p \leq M-1$. Thus, there is N number of operator terms in Eq. (31) of the form defined in Eq. (29). Operator terms involving more than one number operators can be similarly expressed and simplified due to the projection operator in Eq. (31).

Let us now define the *normalized* bosonic creation and annihilation operators

$$\sigma^\dagger |q\rangle_B \equiv |q+1\rangle_B, \quad (32a)$$

$$\sigma |q\rangle_B \equiv |q-1\rangle_B, \quad q > 0 \quad (32b)$$

$$\sigma |0\rangle_B \equiv 0, \quad (32c)$$

which can easily be extended for multimodal systems. The DMS mapping expression for the $p > q$ case consists of Fock projection operators as in Eq. (31) with the $\{\sigma_k^\dagger, \sigma_k\}$ operators. We show an example of the generalized singles excitation mapping with $q = p + 1$ below

$$E_q^{q+1} \mapsto \sigma_1^\dagger \mathcal{C}_{N, q-N+1} + \sum_{k=1}^{N-1} \mathcal{I}_{k-1} \otimes \sum_a \sigma_k \mathcal{P}_{q+a} \otimes \sigma_{k+1}^\dagger \mathcal{C}_{N-k, q-N+k+1}, \quad (33)$$

and state the general expression for the mapping of $\{E_q^p\}$ operators in Appendix C.

As a specific example, let us discuss the DMS operator mapping for the specific case of

$N = 2$ with an arbitrary $M > 2$ number of spin-orbitals. The number operators can be mapped as

$$E_p^p \mapsto \mathbb{I} \otimes |p\rangle \langle p| + \sum_{j+k=p-1} |j, k\rangle \langle j, k|, \quad (34)$$

where $p = 0, 1, \dots, M-1$. The off-diagonal fermionic bilinear operators can be mapped as

$$\begin{aligned} E_q^{q+p} \mapsto & (\sigma_1^\dagger)^p \sum_{j+k=q-1} |j, k\rangle \langle j, k| + \sigma_1^p (\sigma_2^\dagger)^p \sum_j |j+p, q\rangle \langle j+p, q| \\ & - \sum_{j=0}^{p-2} (\sigma_1^\dagger)^{p-2-j} \sigma_1^j (\sigma_2^\dagger)^{j+1} |j, q\rangle \langle j, q|, \end{aligned} \quad (35)$$

where $q = 0, 1, \dots, M-1$ and $p = 1, 2, \dots, M-q-1$. It is also possible to have an alternate representation of the DMS mapping for the $N = 2$ case by applying Eq. (32)

$$E_p^p \mapsto \mathbb{I} \otimes |p\rangle \langle p| + \sum_{j+k=p-1} |j, k\rangle \langle j, k|, \quad (36a)$$

$$\begin{aligned} E_q^{q+p} \mapsto & \sum_{j+k=q-1} |j+p, k\rangle \langle j, k| + \sum_j |j, q+p\rangle \langle j+p, q| \\ & - \sum_{j=0}^{p-2} |p-2-j, q+j+1\rangle \langle j, q|. \end{aligned} \quad (36b)$$

We mention two examples of mapping the number operators below

$$E_0^0 \mapsto \mathbb{I} \otimes |0\rangle \langle 0|, \quad (37a)$$

$$E_1^1 \mapsto \mathbb{I} \otimes |1\rangle \langle 1| + |0, 0\rangle \langle 0, 0|. \quad (37b)$$

Similarly, the off-diagonal bilinear fermionic operators can be mapped, with two examples

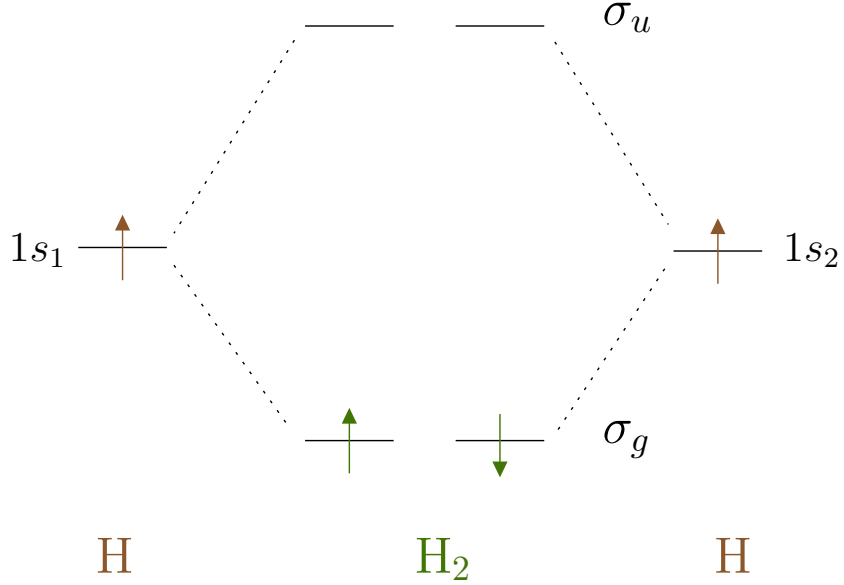


Figure 3: A molecular orbital diagram corresponding to the H_2 molecule in a minimal basis. The molecular orbitals, σ_g and σ_u , are built from $1s$ atomic orbitals of the two hydrogen atoms. In second quantization, the diagram represents the Slater determinant $|0, 1\rangle_F = f_0^\dagger f_1^\dagger |-\rangle_F$, where the first and second spin-orbitals share the σ_g spatial function.

given below

$$E_0^1 \mapsto \sum_{j=1}^L |j-1, 1\rangle \langle j, 0|, \quad (38a)$$

$$E_0^2 \mapsto \left(\sum_{j=1}^{L-1} |j-1, 2\rangle \langle j+1, 0| \right) - |0, 1\rangle \langle 0, 0|, \quad (38b)$$

where we truncated the expansion based on the highest relevant level of the bosonic modes.

4 Simulation of dihydrogen molecule

We apply the ideas discussed above to simulate electronic structure of H_2 molecule here, while also discussing the avenues for generalization to larger molecules.

4.1 Setting up the problem

We discuss the electronic structure of the H_2 molecule in a minimal basis.³² We choose one spatial function per hydrogen atom, which leads to the following molecular spatial orbitals

$$\phi_g = \mathcal{N}_g (1s_1 + 1s_2), \quad (39a)$$

$$\phi_u = \mathcal{N}_u (1s_1 - 1s_2), \quad (39b)$$

where \mathcal{N}_g and \mathcal{N}_u are the normalization factors based on the spatial functions chosen, and one popular choice is the STO-3G minimal basis³⁹ that approximates the Slater-type atomic functions with three real-valued Gaussian functions.³² Having two spatial orbitals means we have an electronic system of two electrons in four spin-orbitals, as shown by the molecular orbital diagram in Figure 3. Let us define the four spin-orbitals as

$$|\chi_0\rangle \equiv |\phi_g, \alpha\rangle, \quad |\chi_1\rangle \equiv |\phi_g, \beta\rangle, \quad (40a)$$

$$|\chi_2\rangle \equiv |\phi_u, \alpha\rangle, \quad |\chi_3\rangle \equiv |\phi_u, \beta\rangle, \quad (40b)$$

where α and β denote spin-orbitals with up and down electron spins, respectively. Then all the possible Slater determinants are

$$|0, 1\rangle_F = f_0^\dagger f_1^\dagger |-\rangle_F, \quad |0, 2\rangle_F = f_0^\dagger f_2^\dagger |-\rangle_F, \quad |0, 3\rangle_F = f_0^\dagger f_3^\dagger |-\rangle_F, \quad (41a)$$

$$|1, 2\rangle_F = f_1^\dagger f_2^\dagger |-\rangle_F, \quad |1, 3\rangle_F = f_1^\dagger f_3^\dagger |-\rangle_F, \quad |2, 3\rangle_F = f_2^\dagger f_3^\dagger |-\rangle_F. \quad (41b)$$

The Fermi vacuum, in this case, is $|0, 1\rangle_F$, the only particle-hole doubles excitation is $|2, 3\rangle_F$, and the rest of the Slater determinants are particle-hole singles excitations with respect to the $|0, 1\rangle_F$ reference.

An arbitrary state in the fermionic Hilbert space can be written as

$$|\Psi\rangle_F = \lambda_1 |0, 1\rangle_F + \lambda_2 |0, 2\rangle_F + \lambda_3 |0, 3\rangle_F + \lambda_4 |1, 2\rangle_F + \lambda_5 |1, 3\rangle_F + \lambda_6 |2, 3\rangle_F, \quad (42)$$

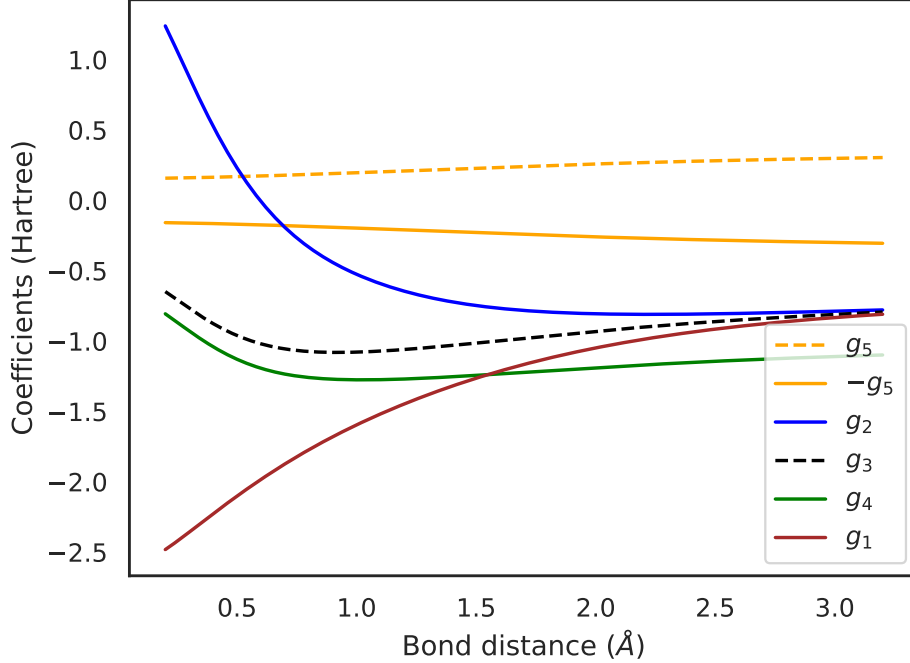


Figure 4: The parametric dependence of the mapped bosonic Hamiltonian coefficients for the dihydrogen molecule in the STO-3G minimal basis, as defined in Eq. (46), on the H–H bond distance. The Hamiltonian coefficients are defined in Table 1.

where $\{\lambda_\mu\}$ are the unknown scalar coefficients, which can be solved, for example, with exact diagonalization to get the exact ground and excited states. We now map the state in Eq. (42) into a bosonic bimodal state by applying Eq. (26) to get

$$|\Psi\rangle_B = \lambda_1 |0, 0\rangle_B + \lambda_2 |1, 0\rangle_B + \lambda_3 |2, 0\rangle_B + \lambda_4 |0, 1\rangle_B + \lambda_5 |1, 1\rangle_B + \lambda_6 |0, 2\rangle_B. \quad (43)$$

Thus, we have managed to represent an arbitrary electronic state of the dihydrogen molecule in terms of basis states of two quantum harmonic oscillator modes.

4.2 Bosonic Hamiltonian

The Hamiltonian of the dihydrogen molecule in a minimal basis can be written as⁸

$$\begin{aligned}
H_F = & h_0^0 f_0^\dagger f_0 + h_1^1 f_1^\dagger f_1 + h_2^2 f_2^\dagger f_2 + h_3^3 f_3^\dagger f_3 + v_{10}^{01} f_0^\dagger f_1^\dagger f_1 f_0 + v_{32}^{23} f_2^\dagger f_3^\dagger f_3 f_2 \\
& + v_{30}^{03} f_0^\dagger f_3^\dagger f_3 f_0 + v_{21}^{12} f_1^\dagger f_2^\dagger f_2 f_1 + (v_{20}^{02} - v_{02}^{02}) f_0^\dagger f_2^\dagger f_2 f_0 + (v_{31}^{13} - v_{13}^{13}) f_1^\dagger f_3^\dagger f_3 f_1 \\
& + v_{12}^{03} (f_0^\dagger f_3^\dagger f_1 f_2 + \text{h.c.}) + v_{32}^{01} (f_0^\dagger f_1^\dagger f_3 f_2 + \text{h.c.}), \tag{44}
\end{aligned}$$

which we want to map to a bosonic form. We first write the Hamiltonian of Eq. (44) in terms of the bilinear fermionic operators

$$\begin{aligned}
H_F = & (h_0^0 + v_{10}^{01} + v_{30}^{03} + v_{20}^{02} - v_{02}^{02}) E_0^0 + (h_1^1 + v_{21}^{12} + v_{31}^{13} - v_{13}^{13}) E_1^1 + (h_2^2 + v_{32}^{23}) E_2^2 + h_3^3 E_3^3 \\
& - v_{10}^{01} E_1^0 E_0^1 - v_{32}^{23} E_3^2 E_2^3 - v_{30}^{03} E_3^0 E_0^3 - v_{21}^{12} E_2^1 E_1^2 - (v_{20}^{02} - v_{02}^{02}) E_2^0 E_0^2 - (v_{31}^{13} - v_{13}^{13}) E_3^1 E_1^3 \\
& - v_{12}^{03} (E_1^0 E_2^3 + \text{h.c.}) - v_{32}^{01} (E_3^0 E_2^1 + \text{h.c.}), \tag{45}
\end{aligned}$$

which means that we need to map the lone operators E_p^p with $p = 0, 1, 2, 3$, the *symmetric* operator couples $E_q^p E_p^q$ with $p = 0, 1, 2$ and $q = p + 1$, and the *transition* operator couples $E_1^0 E_2^3$ and $E_3^0 E_2^1$. The final form of the Hamiltonian mapping of Eq. (45) after applying the DMS mapping of Eq. (36) becomes

$$\begin{aligned}
H_F \mapsto H_B = & g_1 |0, 0\rangle \langle 0, 0| + g_2 |0, 2\rangle \langle 0, 2| + g_3 (|0, 1\rangle \langle 0, 1| + |2, 0\rangle \langle 2, 0|) \\
& + g_4 (|1, 0\rangle \langle 1, 0| + |1, 1\rangle \langle 1, 1|) + g_5 (|0, 0\rangle \langle 0, 2| + \text{h.c.}) \\
& - g_5 (|2, 0\rangle \langle 0, 1| + \text{h.c.}), \tag{46}
\end{aligned}$$

where the scalars $\{g_p\}$ are defined in Table 1. We refer the reader to Appendix D for the intermediate steps in deriving Eq. (46) starting from Eq. (45). The dependence of the bosonic Hamiltonian coefficients of Eq. (46) on the H–H bond distance is shown in Figure 4. The simplification of the bosonic Hamiltonian originates from the fact that the projection

operators should not correspond to a basis state that is outside of Eq. (26) for the dihydrogen molecule. Thus, the bosonic Hamiltonian in Eq. (46) can also be understood as a Hamiltonian of two qutrits, i.e., qudits with three dimensions. The mapped bosonic Hamiltonian has six physical Fock basis states, as mentioned in Eq. (43), and the corresponding matrix heatmap is shown in Figure 5 for the H–H bond distance of 0.7414 Å, which matches exactly with its corresponding fermionic FCI matrix elements.

Let us now discuss the expectation values of the Hamiltonian in Eq. (46) given a bosonic state. There are two classes of operator terms possible for a bosonic Hamiltonian expressed in terms of tensor products of projection operators, namely, the photon counting operator such as $|1, 0\rangle\langle 1, 0|$ and photon transfer operators such as $|2, 0\rangle\langle 0, 1| + \text{h.c.}$. The expectation values for the photon counting operators are easy to interpret. For example, the expectation value of $|1, 0\rangle\langle 1, 0|$ for a given trial state

$$\langle \psi | (|1, 0\rangle\langle 1, 0|) | \psi \rangle = |\langle 1, 0 | \psi \rangle|^2 \quad (47)$$

is equivalent to the probability of measuring one photon in the first and zero photons in the second qumode. The photon counting can be measured by optical detectors in the case of photonic quantum computing,^{40,41} or using cavity-transmon parity measurements in the case of cQED approach.¹²

Computing the expectation value of photon transfer operators can be done via at least two ways. A conceptually straightforward approach involves generalization of the qubit-

Table 1: The bosonic Hamiltonian coefficients of the dihydrogen molecule in a minimal basis defined in Eq. (46) in terms of the one-electron and two-electron integrals defined in Eq. (10).

Coefficient	Definition
g_1	$h_0^0 + h_1^1 + v_{10}^{01}$
g_2	$2h_2^2 + v_{32}^{23}$
g_3	$h_0^0 + h_2^2 + v_{20}^{02}$
g_4	$h_0^0 + h_2^2 + v_{20}^{02} - v_{02}^{02}$
g_5	v_{02}^{02}

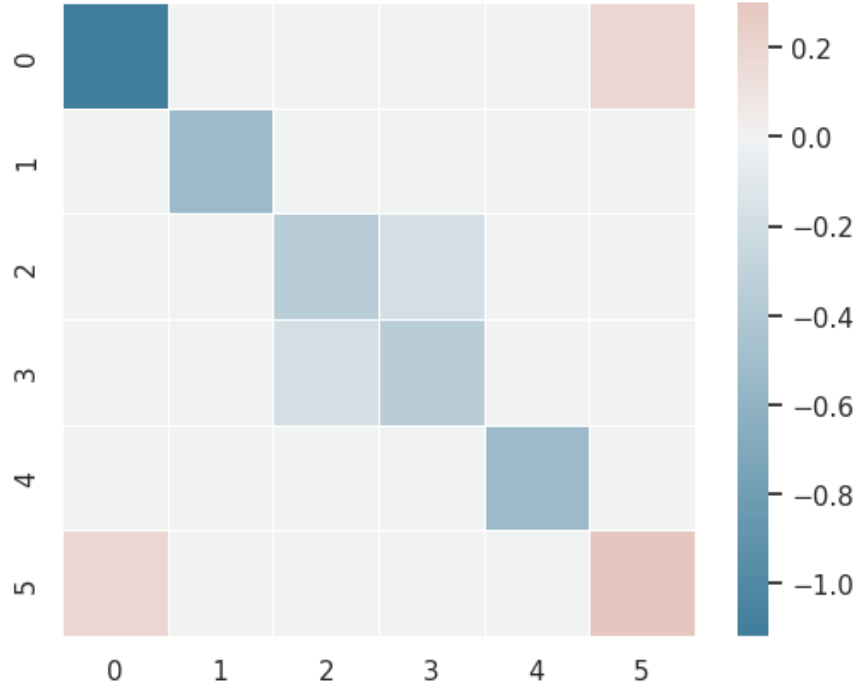


Figure 5: Heatmap of the Hamiltonian matrix elements for the dihydrogen molecule in the STO-3G minimal basis corresponding to the Hamiltonian in Eq. (46) and the FCI state in Eq. (43). The matrix elements are computed for the fixed H–H bond distance of 0.7414 Å and match exactly with their analogous fermionic Hamiltonian matrix elements corresponding to Eq. (45) and Eq. (42).

based Pauli- X operator expectation value for a pairs of qudit states. Let us elaborate with a specific example below

$$\bar{X} \equiv |2, 0\rangle \langle 0, 1| + \text{h.c.} = \bar{H} \bar{Z} \bar{H}, \quad (48)$$

where the generalizations of Pauli- Z and Hadamard operators defined for the relevant qudit subspace are

$$\bar{Z} \equiv |2, 0\rangle \langle 2, 0| - |0, 1\rangle \langle 0, 1|, \quad (49a)$$

$$\bar{H} \equiv \frac{1}{\sqrt{2}} (|2, 0\rangle + |0, 1\rangle) \langle 2, 0| + \frac{1}{\sqrt{2}} (|2, 0\rangle - |0, 1\rangle) \langle 0, 1|. \quad (49b)$$

Since \bar{H} is a unitary operator, expectation value of \bar{X} reduces to photon counting in a rotated

basis

$$\langle \psi | \bar{X} | \psi \rangle = \langle \psi' | \bar{Z} | \psi' \rangle = |\langle 2, 0 | \psi' \rangle|^2 - |\langle 0, 1 | \psi' \rangle|^2, \quad (50)$$

where $|\psi'\rangle = \bar{H} |\psi\rangle$. The expectation values for the other Hamiltonian terms of Eq. (46) can be similarly expressed. The operator \bar{H} can be implemented with a photonic setup,⁴² whereas operators like \bar{H} in cQED approach can be implemented by driving cascaded three-wave or four-wave mixing transitions using a dispersively coupled ancilla qubit, such as $|2, 0, g\rangle \leftrightarrow |0, 0, e\rangle \leftrightarrow |0, 1, g\rangle$, where $|g\rangle$ and $|e\rangle$ represent the ground and excited states of the ancilla.^{43–45} A potentially more scalable approach for computing the expectation value of photon transfer operators between arbitrary multimode Fock states is the recently introduced subspace tomography in cQED,⁴⁶ which does not rely on the \bar{H} operators and instead uses phase space displacement operations that can be implemented efficiently. We refer the reader to Appendix E for more details on the subspace tomography approach.

4.3 Hybrid variational approach

We have all the tools needed for applying a hybrid quantum-classical variational algorithm for finding the ground state energy of the dihydrogen molecule

$$\min_{\psi} E = \frac{\langle \psi | H_B | \psi \rangle}{\langle \psi | \psi \rangle}, \quad (51)$$

where $|\psi\rangle$ is a trial state approximating the bosonic state of Eq. (43) and H_B is the mapped bosonic Hamiltonian in Eq. (46). The hybrid algorithm can assign the computation of the expectation value in Eq. (51) to a bosonic device while the energy function is optimized in a classical processor. Similar to the hybrid algorithms designed for quantum computers with qubits, one needs a robust ansatz for $|\psi\rangle$ for the minimization in Eq. (51). We note that bosonic ansatz has been recently explored for molecular electronic structure, combined with the Jordan–Wigner transformation of the electronic Hamiltonian.⁴⁷

We explore the universal bosonic ansatz of two quomodes for the mapped bosonic Hamil-

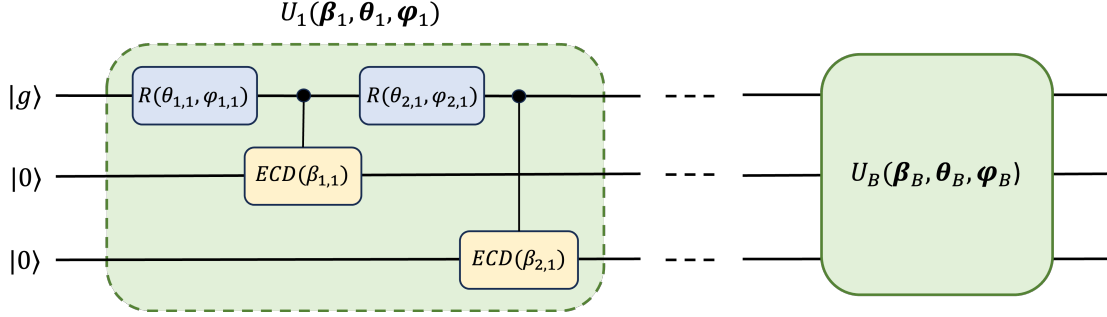


Figure 6: The universal bosonic ansatz for two qumodes with an ancilla qubit, following Ref. 48. The qubit-qumode circuit is initialized in the state $|g\rangle \otimes |0, 0\rangle_B$ and then a block of ECD gates and qubit rotations are acted sequentially, as defined in Eq. (54).

tonian of Eq. (46) here. Universal control of qumodes requires non-Gaussian resources,^{49,50} which in cQED can be provided by the third or higher-order nonlinearity of the ancilla Josephson qubits or couplers.^{51–56} Multiple non-Gaussian elementary gates in cQED can be used to construct a universal gate set, including, most notably, the ancilla-controlled rotation (native for dispersive Hamiltonian),⁵⁷ the selective number-dependent arbitrary phase (SNAP) gate,^{51–53} and the conditional displacement gate.^{48,54} For example, one possible way to implement an arbitrary multi-qumode unitary can be achieved by a sequence of echoed conditional displacement (ECD) gates

$$ECD(\beta) = |e\rangle \langle g| \otimes D(\beta/2) + |g\rangle \langle e| \otimes D(-\beta/2), \quad (52)$$

and ancilla rotations

$$R(\theta, \varphi) = e^{-i\frac{\theta}{2}(\sigma_x \cos \varphi + \sigma_y \sin \varphi)}, \quad (53)$$

where $D(\alpha) = \exp(\alpha b^\dagger - \alpha^* b)$ is the one-qumode displacement operator, $|g\rangle, |e\rangle$ are the ground and excited states of the ancilla qubit, and σ_x, σ_y are the one-qubit Pauli operators.⁴⁸

Thus, a general ansatz for any bosonic Hamiltonian of two qumodes can be written as

$$|\psi\rangle = U_B(\beta_B, \theta_B, \varphi_B) \cdots U_1(\beta_1, \theta_1, \varphi_1) (|g\rangle \otimes |0, 0\rangle_B), \quad (54)$$

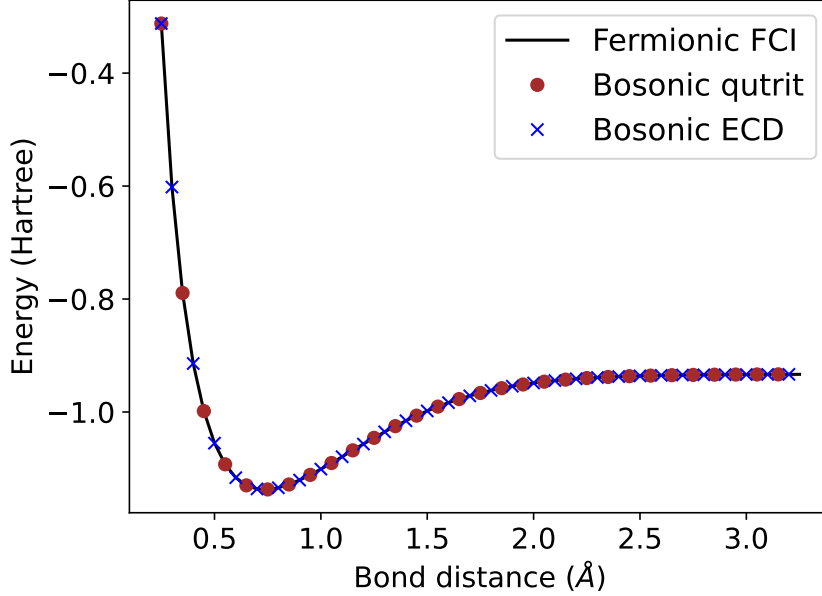


Figure 7: Ground state energies of the dihydrogen molecule in the STO-3G minimal basis for different H–H bond distances. The black line represents the exact energies in the basis of Slater determinants. The brown dots and blue crosses represent the mapped bosonic variational methods described in Section 4.3. Both the bosonic qutrit ansatz (brown dots) and the ECD-rotation ansatz (blue crosses) of Eq. (56) reproduce the exact ground state energies. For the ECD-rotation ansatz, the results are shown for $B = 2$ blocks.

where the initial state for the one ancilla qubit and the two qumodes is $|g, 0, 0\rangle$ and the U_j unitary is defined as

$$\begin{aligned}
 U_j = & \left(|e\rangle \langle g| \otimes \mathbb{I} \otimes D(\beta_{2,j}/2) + |g\rangle \langle e| \otimes \mathbb{I} \otimes D(-\beta_{2,j}/2) \right) \left(R(\theta_{2,j}, \varphi_{2,j}) \otimes \mathbb{I} \otimes \mathbb{I} \right) \\
 & \times \left(|e\rangle \langle g| \otimes D(\beta_{1,j}/2) \otimes \mathbb{I} + |g\rangle \langle e| \otimes D(-\beta_{1,j}/2) \otimes \mathbb{I} \right) \left(R(\theta_{1,j}, \varphi_{1,j}) \otimes \mathbb{I} \otimes \mathbb{I} \right). \quad (55)
 \end{aligned}$$

The two-qumode ansatz of Eq. (54) has B number of U_j blocks and is illustrated in Figure 6. The strategy of using an ancilla qubit rotation and ECD gates can be similarly extended for any number of qumodes.⁴⁸ Additional strategies for multi-mode control such as based on the conditional-NOT displacement⁵⁶ and photon blockade⁵⁵ have also been demonstrated recently.

Specifically for the ground state of H_2 molecule in a minimal basis, the only relevant Slater determinant basis states are $|0, 1\rangle_F$ and $|2, 3\rangle_F$,⁵⁸ which becomes the qumode Fock basis states $|0, 0\rangle_B$ and $|0, 2\rangle_B$ after the state mapping. This means the general ansatz of Eq. (54) can be applied to find the ground state of H_2 molecule, even without optimizing the parameters on the first qumode. In that case, the following reduced version of Eq. (54) is sufficient for the ground state of H_2 molecule⁵⁴

$$|\psi\rangle = U_B(\beta_B, \theta_B, \varphi_B) \cdots U_1(\beta_1, \theta_1, \varphi_1) (|g\rangle \otimes |0, 0\rangle_B), \quad (56a)$$

$$U_j = \left(|e\rangle\langle g| \otimes \mathbb{I} \otimes D(\beta_j/2) + |g\rangle\langle e| \otimes \mathbb{I} \otimes D(-\beta_j/2) \right) \left(R(\theta_j, \varphi_j) \otimes \mathbb{I} \otimes \mathbb{I} \right), \quad (56b)$$

where B is the number of blocks and $\{\beta_j, \theta_j, \varphi_j\}$ needs to be optimized following Eq. (51). As shown in Figure 7, the ECD-rotation ansatz of Eq. (56) with only $B = 2$ blocks can reproduce the exact ground state energies for different H–H bond distances. Since the H_B defined in Eq. (46) can be thought of as a Hamiltonian of two qutrits, starting from the initial state $|0, 0\rangle_B$ and applying $e^{-2i\theta} (-i|0\rangle\langle 2| + \text{h.c.})$, which is a qutrit R_y gate,^{59,60} to the second qumode is also an legitimate ansatz for the ground state, where the scalar θ is optimized following Eq. (51). As shown in Figure 7, both the general ECD-rotation and the qutrit ansatz can reach the exact ground state energies of the H_2 molecule. It is important to note that the expectation value of H_B for any Fock basis state that is absent in H_B is naturally zero, which allows the design of flexible bosonic ansatz without contaminating the trial energy in Eq. (51), while potentially boosting the optimization.

5 Conclusions

We have introduced a general scheme for mapping the molecular electronic structure Hamiltonian in terms of projection operators of quantum harmonic oscillators or qumodes based on an exact fermion to boson operator map that in turn is derived from a state mapping between Slater determinants and Fock states of qumodes. Our work opens the door for

simulating molecular electronic structure, and by extension, any number-conserving many-fermion system, on bosonic quantum devices that use qumodes as the building blocks of quantum information.

After mapping the fermionic Hamiltonian to a qumode Hamiltonian, one can consider the electronic structure of interest as a bosonic problem and apply a bosonic ansatz as the trial state for variationally finding the ground state using a classical-quantum hybrid approach. This is related in spirit to the qubit coupled cluster approach, where a hardware-efficient qubit ansatz is used after mapping the electronic structure Hamiltonian to a qubit Hamiltonian.⁶¹ We have applied the techniques discussed above to the dihydrogen molecule in a minimal basis, a system of two electrons that is mapped to a system of two qumodes. We have shown how to compute the expectation values using bosonic quantum devices, and shown that a minimal bosonic ansatz reproduces the exact energies for the potential energy surface of the H₂ molecule.

For a general electronic structure Hamiltonian of N electrons with M spin-orbitals, one needs N number of qumodes with $M - N + 1$ number of accessible excitation levels. The computation of the Hamiltonian expectation value needs to take care of a maximum of $\mathcal{O}(M^4 N^2)$ number of operator terms compared to a maximum of $\mathcal{O}(M^4)$ number of terms in the case of the traditional qubit-based approaches. However, the number of Hamiltonian terms can potentially be reduced by applying tensor decomposition techniques to the one-electron and two-electron integrals.^{62,63} Thus, scaling up the fermion to boson mapping techniques discussed here for larger molecular systems is an exciting challenge, and we hope that the present work inspires a new generation of algorithms for electronic structure theory that harness the unique capabilities of bosonic quantum devices.

Acknowledgement

We acknowledge support from the NSF for the Center for Quantum Dynamics on Modular Quantum Devices (CQD-MQD) under grant number CHE-2124511.

A Justification of the state mapping

The state mapping in Eq. (20) is justified if we can prove that acting with bosonic operators $\{b_j^\dagger, b_j\}$ on the mapped fermionic states still preserve their commutation relations of Eq. (17). We follow the derivation done in Ref. 30 here, although a similar justification was first given by Ref. 29.

The first step to deduce the action of bosonic creation operators on a Slater determinant is to apply Eq. (20) and Eq. (18) to get

$$b_j^\dagger |p_1, \dots, p_N\rangle_F = b_j^\dagger |q_1, \dots, q_N\rangle_B = \sqrt{q_j + 1} |q_1, \dots, q_j + 1, \dots, q_N\rangle_B, \quad (57)$$

which can be again mapped back to

$$b_j^\dagger |p_1, \dots, p_N\rangle_F = \sqrt{p_{N-j+1} - p_{N-j}} |p_1, \dots, p_{N-k}, p_{N-k+1} + 1, \dots, p_N + 1\rangle_F, \quad (58)$$

where $j < N$. The same expression for the special case of $j = N$ is given by

$$b_N^\dagger |p_1, \dots, p_N\rangle_F = \sqrt{p_1 + 1} |p_1 + 1, \dots, p_N + 1\rangle_F, \quad (59)$$

The action of bosonic annihilation operators on a Slater determinant can be similarly derived as

$$b_j |p_1, \dots, p_N\rangle_F = \sqrt{p_{N-j+1} - p_{N-j} - 1} |p_1, \dots, p_{N-k}, p_{N-k+1} - 1, \dots, p_N - 1\rangle_F, \quad (60)$$

when $j < N$ and

$$b_N |p_1, \dots, p_N\rangle_F = \sqrt{p_1} |p_1 - 1, \dots, p_N - 1\rangle_F. \quad (61)$$

Let us now combine Eq. (58) and Eq. (60) to arrive at

$$\begin{aligned} b_j b_k^\dagger |p_1, \dots, p_N\rangle_F &= \sqrt{(p_{N-k+1} - p_{N-k})(p_{N-j+1} - p_{N-j} - 1)} \\ &\times |p_1, \dots, p_{N-k}, p_{N-k+1} + 1, \dots, p_{N-j} + 1, p_{N-j+1}, \dots, p_N\rangle_F, \end{aligned} \quad (62)$$

where $j < k$. Similarly, by reversing the order of the bosonic operators, we get

$$\begin{aligned} b_k^\dagger b_j |p_1, \dots, p_N\rangle_F &= \sqrt{(p_{N-k+1} - p_{N-k})(p_{N-j+1} - p_{N-j} - 1)} \\ &\times |p_1, \dots, p_{N-k}, p_{N-k+1} + 1, \dots, p_{N-j} + 1, p_{N-j+1}, \dots, p_N\rangle_F, \end{aligned} \quad (63)$$

where $j < k$. Thus, the right hand sides of Eq. (62) and Eq. (63) are the same, which proves $[b_j, b_k^\dagger] = 0$ for $j < k$. The $j > k$ case can be similarly derived as above. Let us now consider the $j = k$ case

$$b_k b_k^\dagger |p_1, \dots, p_N\rangle_F = (p_{N-k+1} - p_{N-k}) |p_1, \dots, p_N\rangle_F. \quad (64)$$

Similarly, by reversing the order, we get

$$b_k^\dagger b_k |p_1, \dots, p_N\rangle_F = (p_{N-k+1} - p_{N-k} - 1) |p_1, \dots, p_N\rangle_F. \quad (65)$$

Thus, Eq. (64) and Eq. (65) shows that $[b_k, b_k^\dagger] = 1$, which proves that the state mapping preserves the relation $[b_j, b_k^\dagger] = \delta_{jk}$.

B Derivation of the operator mapping

The derivation of the mapping $\{E_q^p\}$ operators is shown in Ref. 30. We gain insight into the derivation here by discussing all the steps for the specific cases of $N = 1$ and $N = 2$.

Let us first discuss the operator mapping with an $N = 1$ system. The state mapping is then simply $|j\rangle_F \leftrightarrow |j\rangle_B$, where the one-particle states are defined as

$$|j\rangle_F \equiv f_j^\dagger |-\rangle_F, \quad |j\rangle_B \equiv \frac{b_j^\dagger}{\sqrt{j!}} |0\rangle_B. \quad (66)$$

Let us figure out how the bilinear fermionic operators act on the state $|j\rangle_B$ by using the state mapping. The states $\{|j\rangle_F\}$ are eigenstate of the number operator E_p^p , and combining this with the state mapping leads to

$$E_p^p |j\rangle_F = \delta_{pj} |j\rangle_B = (|j\rangle \langle p|) |j\rangle_B = (|p\rangle \langle p|) |j\rangle_B, \quad (67)$$

where $|p\rangle \langle p|$ is the projection operator in the bosonic Fock basis with the subscripts ‘‘B’’ suppressed to avoid symbolic clutter. Since $|j\rangle_B$ can now be mapped back to $|j\rangle_F$, the number operator is thus mapped as

$$E_p^p \mapsto |p\rangle \langle p|, \quad (68)$$

$p = 0, 1, \dots, M - 1$. Similarly, acting with the off-diagonal bilinear fermionic operator on $|j\rangle_F$ leads to

$$E_{q+p}^q |j\rangle_F = \delta_{qj} f_{j+p}^\dagger |-\rangle_F = \delta_{qj} |j+p\rangle_F, \quad (69)$$

which maps to the state $|j+p\rangle_B$. We can now combine Eq. (69) and Eq. (32) to arrive at

$$E_q^{q+p} |j\rangle_F = (\sigma^\dagger)^p \delta_{q,j} |j\rangle_B = (\sigma^\dagger)^p (|q\rangle \langle q|) |j\rangle_B. \quad (70)$$

Since $|j\rangle_B$ can now be mapped back to $|j\rangle_F$, the E_q^{q+p} operator can be mapped as

$$E_q^{q+p} \mapsto (\sigma^\dagger)^p |q\rangle \langle q|, \quad (71)$$

where $q = 1, \dots, M-1$ and $p = 1, \dots, M-p-1$. Because of its adjoint relation $(E_q^p)^\dagger = E_p^q$, mapping bilinear fermionic operators $\{E_q^p\}$ for $p \geq q$ is sufficient.

Let us now discuss the $N = 2$ case, for which the state mapping is given by, $|p, q\rangle_F \leftrightarrow |j, k\rangle_B$, where the states are defined in Eq. (23) and Eq. (24), and the relation between the two sets of indices are given by Eq. (25). Let us start our derivation by writing down how the number operator E_r^r acts on an arbitrary Slater determinant

$$E_r^r |p, q\rangle_F = (\delta_{p,r} + \delta_{q,r}) |p, q\rangle_F, \quad (72)$$

and after applying the state mapping back and forth, we arrive at

$$\begin{aligned} E_r^r |p, q\rangle_F &\mapsto (\delta_{k,r} + \delta_{j+k,r-1}) |j, k\rangle_B \\ &= \left[\delta_{k,r} + \sum_{a+b=r-1} \delta_{j,a} \delta_{k,b} \right] |j, k\rangle_B \\ &= \left[\mathbb{I} \otimes |r\rangle \langle r| + \sum_{a+b=r-1} |a, b\rangle \langle a, b| \right] |j, k\rangle_B \\ &\mapsto \left[\mathbb{I} \otimes |r\rangle \langle r| + \sum_{a+b=r-1} |a, b\rangle \langle a, b| \right] |p, q\rangle_F, \end{aligned} \quad (73)$$

where \mathbb{I} is the identity operator acting on the first mode. We extended the projection operator trick in the derivation of the $N = 1$ system here, i.e., the goal is to find a Kronecker delta involving one of the indices (j and k) corresponding to the two modes. We can now redefine the dummy indices above and express the mapping for the number operators as

$$E_p^p \mapsto \mathbb{I} \otimes |p\rangle \langle p| + \sum_{a+b=p-1} |a, b\rangle \langle a, b|. \quad (74)$$

Let us now map the off-diagonal operators. We first act E_s^{s+r} on an arbitrary Slater determinant

$$E_s^{s+r} |p, q\rangle_F = \delta_{p,s} f_{p+r}^\dagger f_q^\dagger |-\rangle_F + \delta_{q,s} f_p^\dagger f_{q+r}^\dagger |-\rangle_F, \quad (75)$$

which can be further written as

$$\begin{aligned}
E_s^{s+r} |p, q\rangle_F &= \delta_{p,s} \left(\sum_{a=p+1}^{q-1} \delta_{p+r,a} |p+r, q\rangle_F - \sum_{a=q+1}^{\infty} \delta_{p+r,a} |q, p+r\rangle_F \right) \\
&\quad + \delta_{q,s} |p, q+r\rangle_F,
\end{aligned} \tag{76}$$

where we have applied the definition of Slater determinants in Eq. (8). Similar to the derivation for the $N = 1$ case, we now apply the state mapping and the normalized bosonic operators. The third term of Eq. (76) then reduces to

$$\delta_{q,s} |p, q+r\rangle_F \mapsto \delta_{j+k, s-1} |j+r, k\rangle_B = (\sigma_1^\dagger)^r \delta_{j+k, s-1} |j, k\rangle_B, \tag{77}$$

Similarly the first term of Eq. (76) can be rewritten as

$$\begin{aligned}
\delta_{p,s} \sum_{a=p+1}^{q-1} \delta_{p+r,a} |p+r, q\rangle_F &\mapsto \delta_{p,s} \sum_{a=p+1}^{q-1} \delta_{p+r,a} |j-r, k+r\rangle_B \\
&= \sigma_1^r (\sigma_2^\dagger)^r \sum_{a=0}^{\infty} \delta_{j, r+a} \delta_{k, s} |j, k\rangle_B,
\end{aligned} \tag{78}$$

whereas the second term of Eq. (76) turns to

$$\begin{aligned}
\delta_{p,s} \sum_{a=q+1}^{\infty} \delta_{p+r,a} |q, p+r\rangle_F &\mapsto \delta_{p,s} \sum_{a=0}^{\infty} \delta_{p+r, a+q+1} |r-2-j, j+k+1\rangle_B \\
&= \sum_{a=0}^{r-2} (\sigma_1^\dagger)^{r-2-a} \sigma_1^a (\sigma_2^\dagger)^{a+1} \delta_{j,a} \delta_{k,s} |j, k\rangle_B.
\end{aligned} \tag{79}$$

Applying the projection operator relation and the state mapping back to the Slater determinants, the action of the E_s^{s+r} on an arbitrary Slater determinant can now be written

as

$$\begin{aligned}
E_s^{s+r} |p, q\rangle_F &= \left[\sigma_1^r (\sigma_2^\dagger)^r \sum_{a=0}^{\infty} |r+a, s\rangle \langle r+a, s| - \sum_{a=0}^{r-2} (\sigma_1^\dagger)^{r-2-a} \sigma_1^a (\sigma_2^\dagger)^{a+1} |a, s\rangle \langle a, s| \right. \\
&\quad \left. + (\sigma_1^\dagger)^r \sum_{a+b=s-1} |a, b\rangle \langle a, b| \right] |p, q\rangle_F. \tag{80}
\end{aligned}$$

We can now redefine the dummy indices above and express the mapping for the off-diagonal operators as

$$\begin{aligned}
E_q^{q+p} &\mapsto \sigma_1^p (\sigma_2^\dagger)^p \sum_{a=0}^{\infty} |p+a, q\rangle \langle p+a, q| - \sum_{a=0}^{p-2} (\sigma_1^\dagger)^{p-2-a} \sigma_1^a (\sigma_2^\dagger)^{a+1} |a, q\rangle \langle a, q| \\
&\quad + (\sigma_1^\dagger)^p \sum_{a+b=q-1} |a, b\rangle \langle a, b|. \tag{81}
\end{aligned}$$

Thus, we have shown how to derive the DMS operator mapping for the $N = 1$ and $N = 2$ cases.

C General DMS mapping expression

The expression for the DMS mapping of $\{E_q^p\}$ with $p > q$ is given by³⁰

$$\begin{aligned}
E_q^{q+p} \mapsto & \sum_{\substack{r_1+\dots+r_N \\ = q-N+1}} (\sigma_1^\dagger)^p \mathcal{P}_{r_1, \dots, r_N} + \sum_{a=0}^{\infty} \sum_{\substack{r_2+\dots+r_N \\ = q-N+2}} \sigma_1^p (\sigma_2^\dagger)^p \mathcal{P}_{p+a, r_2, \dots, r_N} \\
& - \sum_{\mu=0}^{p-2} \sum_{\substack{r_2+\dots+r_N \\ = q-N+2}} (\sigma_1^\dagger)^{p-2-\mu} \sigma_1^\mu (\sigma_2^\dagger)^{\mu+1} \mathcal{P}_{\mu, r_2, \dots, r_N} \\
& + \sum_{k=2}^{N-1} \left[\mathcal{I}_{k-1} \otimes \sum_{a=0}^{\infty} \sum_{\substack{r_{k+1}+\dots+r_N \\ = q-N+k+1}} \sigma_k^p (\sigma_{k+1}^\dagger)^p \mathcal{P}_{p+a, r_{k+1}, \dots, r_N} \right. \\
& - \mathcal{I}_{k-2} \otimes \sum_{a=0}^{\infty} \sum_{\mu=0}^{p-2} \sum_{r_{k-1}=a+1}^{p+a-1} \sum_{\substack{r_{k+1}+\dots+r_N \\ = q-N+k+1}} \mathcal{T}_{p,k,\mu}^1 \mathcal{P}_{r_{k-1}, \mu, r_{k+1}, \dots, r_N} \\
& + (-1)^k \left(\sum_{r_1=0}^{\infty} \dots \sum_{r_k=0}^{\infty} - \sum_{a=0}^{\infty} \sum_{\substack{r_1+\dots+r_k \\ = p+a-k}} \right) \sum_{\substack{r_{k+1}+\dots+r_N \\ = q-N+k+1}} \mathcal{T}_{p,k,\mu_1, \dots, \mu_k}^2 \mathcal{P}_{r_1, \dots, r_N} \\
& + \sum_{j=2}^{k-1} (-1)^j \mathcal{I}_{k-j-1} \otimes \sum_{a=0}^{\infty} \left(\sum_{\substack{r_{k-j}+\dots+r_k \\ = p+a-j}} \sum_{\substack{r_{k+1}+\dots+r_N \\ = q-N+k+1}} \mathcal{T}_{p,k,j,r_{k-j+1}, \dots, r_k}^3 \mathcal{P}_{r_{k-j}, \dots, r_N} \right. \\
& \left. - \sum_{\substack{r_{k-j+1}+\dots+r_k \\ = p+a-j}} \sum_{\substack{r_{k+1}+\dots+r_N \\ = q-N+k+1}} \mathcal{T}_{p,k,j,r_{k-j+1}, \dots, r_k}^3 |0\rangle \langle 0| \otimes \mathcal{P}_{r_{k-j+1}, \dots, r_N} \right) \Big], \tag{82}
\end{aligned}$$

where $q = 0, \dots, M-2$ and $p = 1, \dots, M-q-1$ and the operators $\{\mathcal{T}^\mu\}$ are defined in Table 2. All the summations in Eq. (82) will naturally truncate following the highest Fock state allowed for a qumode based on the state mapping of Eq. (21). There are $\mathcal{O}(N^2)$ number of terms in Eq. (82) that need to be taken care of in case of computing the expectation value of the operator E_q^{q+p} . The expression for $\{E_q^p\}$ with $p < q$ can be found by taking the Hermitian conjugate of Eq. (82), while the mapping for $p = q$ is given by Eq. (31).

D Derivation of the bosonic Hamiltonian for the dihydrogen molecule

Let us map each of the operator terms of the Hamiltonian in Eq. (45). The maps corresponding to the operator terms with single bilinear fermionic operators are given following Eq. (34)

$$E_0^0 \mapsto \mathbb{I} \otimes |0\rangle \langle 0|, \quad (83a)$$

$$E_1^1 \mapsto \mathbb{I} \otimes |1\rangle \langle 1| + |0, 0\rangle \langle 0, 0|, \quad (83b)$$

$$E_2^2 \mapsto \mathbb{I} \otimes |2\rangle \langle 2| + |0, 1\rangle \langle 0, 1| + |1, 0\rangle \langle 1, 0|, \quad (83c)$$

$$E_3^3 \mapsto |0, 2\rangle \langle 0, 2| + |1, 1\rangle \langle 1, 1| + |2, 0\rangle \langle 2, 0|, \quad (83d)$$

where we have truncated the mapping expression based on the relevant bosonic subspace for our problem. The expressions after mapping the symmetric operator terms using Eq. (36)

Table 2: Definitions for the intermediate operator terms used in Eq. (82).

Operator	Definition
$\mathcal{T}_{p,k,\mu}^1$	$\sigma_{k-1}^{p-1-\mu} (\sigma_k^\dagger)^{p-2-\mu} \sigma_k^\mu (\sigma_{k+1}^\dagger)^{\mu+1}$
$\mathcal{T}_{p,k,r_1,\dots,r_k}^2$	$(\sigma_1^\dagger)^{p-1-k-(r_1+\dots+r_k)} \sigma_1^{r_1} (\sigma_2^\dagger)^{r_1} \dots \sigma_{k-1}^{r_{k-1}} (\sigma_k^\dagger)^{r_{k-1}} \sigma_k^{r_k} (\sigma_{k+1}^\dagger)^{r_k+1}$
$\mathcal{T}_{p,k,j,\mu_{k-j+1},\dots,\mu_k}^3$	$\sigma_{k-j}^{p-j-(\mu_{k-j+1}+\dots+\mu_k)} (\sigma_{k-j+1}^\dagger)^{p-j-1-(\mu_{k-j+1}+\dots+\mu_k)}$ $\times \sigma_{k-j+1}^{\mu_{k-j+1}} (\sigma_{k-j+2}^\dagger)^{\mu_{k-j+1}} \dots \sigma_{k-1}^{\mu_{k-1}} (\sigma_k^\dagger)^{\mu_{k-1}} \sigma_k^{\mu_k} (\sigma_{k+1}^\dagger)^{\mu_k+1}$

are

$$E_1^0 E_0^1 \mapsto |1, 0\rangle \langle 1, 0| + |2, 0\rangle \langle 2, 0|, \quad (84a)$$

$$E_3^0 E_0^3 \mapsto |0, 0\rangle \langle 0, 0| + |1, 0\rangle \langle 1, 0|, \quad (84b)$$

$$E_2^1 E_1^2 \mapsto |0, 0\rangle \langle 0, 0| + |1, 1\rangle \langle 1, 1| + |2, 1\rangle \langle 2, 1|, \quad (84c)$$

$$E_2^0 E_0^2 \mapsto |0, 0\rangle \langle 0, 0| + |2, 0\rangle \langle 2, 0|, \quad (84d)$$

$$E_3^1 E_1^3 \mapsto |0, 0\rangle \langle 0, 0| + |0, 1\rangle \langle 0, 1| + |2, 1\rangle \langle 2, 1|, \quad (84e)$$

$$E_3^2 E_2^3 \mapsto |0, 1\rangle \langle 0, 1| + |1, 0\rangle \langle 1, 0| + |1, 2\rangle \langle 1, 2| + |2, 2\rangle \langle 2, 2|. \quad (84f)$$

The rest of the operator terms are similarly mapped as

$$E_1^0 E_2^3 \mapsto |2, 0\rangle \langle 0, 1|, \quad (85a)$$

$$E_3^0 E_2^1 \mapsto -|0, 0\rangle \langle 0, 2|. \quad (85b)$$

We now combine Eq. (83), Eq. (84), and Eq. (85) to arrive at

$$\begin{aligned} H_B = & \left(h_0^0 + h_1^1 + v_{10}^{01} \right) |0, 0\rangle \langle 0, 0| + \left(h_1^1 + h_2^2 + v_{21}^{12} \right) |0, 1\rangle \langle 0, 1| \\ & + \left(h_0^0 + h_2^2 + v_{20}^{02} - v_{02}^{02} \right) |1, 0\rangle \langle 1, 0| + \left(h_1^1 + h_3^3 + v_{31}^{13} - v_{13}^{13} \right) |1, 1\rangle \langle 1, 1| \\ & + \left(h_2^2 + h_3^3 + v_{32}^{23} \right) |0, 2\rangle \langle 0, 2| + \left(h_0^0 + h_3^3 + v_{30}^{03} \right) |2, 0\rangle \langle 2, 0| \\ & + v_{32}^{01} (|0, 0\rangle \langle 0, 2| + \text{h.c.}) - v_{12}^{03} (|2, 0\rangle \langle 0, 1| + \text{h.c.}). \end{aligned} \quad (86)$$

We can simplify even more by taking advantage of the symmetries of the four spin-orbitals of the H₂ molecule in a minimal basis, which leads to the following relations⁸

$$h_0^0 = h_1^1, \quad (87a)$$

$$h_2^2 = h_3^3, \quad (87b)$$

$$v_{20}^{02} = v_{31}^{13} = v_{21}^{12} = v_{30}^{03}, \quad (87c)$$

$$v_{02}^{02} = v_{12}^{03} = v_{32}^{01} = v_{13}^{13}. \quad (87d)$$

Thus, we can finally map the Hamiltonian in Eq. (45) to the bosonic form below

$$\begin{aligned} H_B = & \left(h_0^0 + h_1^1 + v_{10}^{01} \right) |0, 0\rangle \langle 0, 0| + \left(h_0^0 + h_2^2 + v_{20}^{02} \right) |0, 1\rangle \langle 0, 1| \\ & + \left(h_0^0 + h_2^2 + v_{20}^{02} - v_{02}^{02} \right) |1, 0\rangle \langle 1, 0| + \left(h_0^0 + h_2^2 + v_{20}^{02} - v_{02}^{02} \right) |1, 1\rangle \langle 1, 1| \\ & + \left(2h_2^2 + v_{32}^{23} \right) |0, 2\rangle \langle 0, 2| + \left(h_0^0 + h_2^2 + v_{20}^{02} \right) |2, 0\rangle \langle 2, 0| \\ & + v_{02}^{02} (|0, 0\rangle \langle 0, 2| + \text{h.c.}) - v_{02}^{02} (|2, 0\rangle \langle 0, 1| + \text{h.c.}), \end{aligned} \quad (88)$$

which is equivalent to the Hamiltonian in Eq. (46).

E Subspace tomography for computing photon transfer expectation values

The cQED-based subspace tomography approach described in Ref. 46 can be implemented with the help of an ancilla transmon qutrit and can be divided into two broad parts. Let us denote the three levels of the ancilla to be $|g\rangle$, $|e\rangle$, and $|f\rangle$. The first part uses a unitary operator coupled to the states $|e, g\rangle$ that transforms the full density matrix of a qumode state into a chosen subspace density matrix coupled to the $|e\rangle$ state. The second part applies phase displacement operator(s) followed by a photon-number state projection and measure the corresponding probability in the $|f\rangle$ state. We discuss the resulting expressions below.

Let us first understand the above protocol for one qumode, whose state can be represented in the Fock basis as

$$|\Psi\rangle = \sum_{n=0}^{\infty} C_n |n\rangle, \quad (89)$$

where $\{C_n\}$ are the complex-valued Fock basis coefficients. Let us assume we want to compute the expectation value of the following photon transfer operator $|j\rangle\langle k| + \text{h.c.}$

$$T_{j,k} = \langle\Psi|(|j\rangle\langle k| + \text{h.c.})|\Psi\rangle = C_j C_k^* + C_k C_j^*, \quad (90)$$

where the operator pairing for the off-diagonal parts ensure Hermiticity. The subspace tomography approach will choose to handle the corresponding subspace density matrix

$$\rho_{j,k} = \left(\sum_{n=j,k} C_n |n\rangle \right) \left(\sum_{n=j,k} C_n^* \langle n| \right) = \sum_{n,m \in \mathcal{S}} C_n C_m^* |n\rangle \langle m|, \quad (91)$$

where \mathcal{S} represent the subspace chosen. Let us now apply the phase space displacement operator $D(\alpha) = e^{\alpha b^\dagger - \alpha^* b}$, which creates all possible photon excitation and deexcitation from the Fock state it acts on

$$D(\alpha) |n\rangle = \sum_{j=0}^{\infty} d_{n,j} |j\rangle, \quad (92)$$

where $\{d_{n,j}\}$ are the known and easily tunable linear coefficients associated with the displacement operator. The displacement operator transforms $\rho_{j,k}$ as

$$\begin{aligned} R_{j,k}^{(1)} &\equiv D(\alpha) \rho_{j,k} D^\dagger(\alpha) \\ &= \sum_{n,m \in \mathcal{S}} C_n C_m^* \left[D(\alpha) |n\rangle \langle m| D^\dagger(\alpha) \right] \\ &= \sum_{n,m \in \mathcal{S}} C_n C_m^* \sum_{j,k \in \mathbb{N}} d_{n,j} (d_{m,k})^* |j\rangle \langle k|. \end{aligned} \quad (93)$$

The final observable can now be represented as

$$R_{j,k,p}^{(2)} \equiv \text{Tr}(|p\rangle \langle p| R_{j,k}^{(1)} |p\rangle \langle p|) = \sum_{n,m \in \mathcal{S}} C_n C_m^* d_{n,p} (d_{m,p})^*. \quad (94)$$

Assuming all $\{d_{n,p}\}$ coefficients to be real-valued, Eq. (94) can be rewritten as

$$\begin{aligned} R_{j,k,p}^{(2)} &= \sum_{n,m \in \mathcal{S}} d_{n,p} d_{m,p} C_n C_m^* \\ &= d_{j,p} d_{j,p} C_j C_j^* + d_{k,p} d_{k,p} C_k C_k^* + d_{j,p} d_{k,p} (C_j C_k^* + C_k C_j^*) \\ &= d_{j,p}^2 |\langle j|\Psi\rangle|^2 + d_{k,p}^2 |\langle k|\Psi\rangle|^2 + d_{j,p} d_{k,p} T_{j,k}. \end{aligned} \quad (95)$$

Since $R_{j,k,p}^{(2)}$ is the observable for the subspace tomography and $\{|\langle j|\Psi\rangle|^2\}$ can be computed by photon number counting as discussed in Section 4.2, the expectation value for the photon transfer operator can be computed as

$$T_{j,k} = \frac{1}{d_{j,p} d_{k,p}} \left(R_{j,k,p}^{(2)} - d_{j,p}^2 |\langle j|\Psi\rangle|^2 - d_{k,p}^2 |\langle k|\Psi\rangle|^2 \right). \quad (96)$$

The generalization of the above approach to N number of qumodes is straightforward with one phase space displacement operators acting on each of the qumodes. In this case, we want to compute the expectation value of the photon transfer operator

$$T_{\mathbf{j},\mathbf{k}} = \langle \Psi | (|\mathbf{j}\rangle \langle \mathbf{k}| + \text{h.c.}) | \Psi \rangle, \quad (97)$$

where \mathbf{j} is a vector of natural numbers and $|\mathbf{j}\rangle \equiv |j_1, \dots, j_N\rangle_B$ is a bosonic Fock state. The corresponding subspace density matrix is

$$\rho_{\mathbf{j},\mathbf{k}} = \left(\sum_{\mathbf{n}=\mathbf{j},\mathbf{k}} C_{\mathbf{n}} |\mathbf{n}\rangle \right) \left(\sum_{\mathbf{n}=\mathbf{j},\mathbf{k}} C_{\mathbf{n}}^* \langle \mathbf{n}| \right) = \sum_{\mathbf{n},\mathbf{m} \in \mathcal{S}} C_{\mathbf{n}} C_{\mathbf{m}}^* |\mathbf{n}\rangle \langle \mathbf{m}|, \quad (98)$$

and the experimental observables are

$$R_{\mathbf{j},\mathbf{k}}^{(1)} \equiv D_N(\alpha) \cdots D_1(\alpha) \rho_{\mathbf{j},\mathbf{k}} D_1^\dagger(\alpha) \cdots D_N^\dagger(\alpha), \quad (99a)$$

$$R_{\mathbf{j},\mathbf{k},\mathbf{p}}^{(2)} \equiv \text{Tr}(|\mathbf{p}\rangle \langle \mathbf{p}| R_{\mathbf{j},\mathbf{k}}^{(1)} |\mathbf{p}\rangle \langle \mathbf{p}|), \quad (99b)$$

where $D_p(\alpha)$ is the displacement operator acting on the p -th qumode and $|\mathbf{p}\rangle \langle \mathbf{p}|$ is the multimode projection operator. Similar to discussion above, $T_{\mathbf{j},\mathbf{k}}$ can then be expressed as

$$T_{\mathbf{j},\mathbf{k}} = \frac{1}{\prod_{i=1}^N d_{j_i,p_i} d_{k_i,p_i}} \left[R_{\mathbf{j},\mathbf{k},\mathbf{p}}^{(2)} - \left(\prod_{i=1}^N d_{j_i,p_i}^2 \right) |\langle \mathbf{j} | \Psi \rangle|^2 - \left(\prod_{i=1}^N d_{k_i,p_i}^2 \right) |\langle \mathbf{k} | \Psi \rangle|^2 \right]. \quad (100)$$

Thus, it is possible to compute the expectation value of any photon transfer operator of the form $|\mathbf{j}\rangle \langle \mathbf{k}| + \text{h.c.}$ using the subspace tomography approach.

References

- (1) Vogiatzis, K. D.; Ma, D.; Olsen, J.; Gagliardi, L.; De Jong, W. A. Pushing configuration-interaction to the limit: Towards massively parallel MCSCF calculations. *J. Chem. Phys.* **2017**, *147*, 184111.
- (2) Peruzzo, A.; McClean, J.; Shadbolt, P.; Yung, M.-H.; Zhou, X.-Q.; Love, P. J.; Aspuru-Guzik, A.; O'Brien, J. L. A Variational Eigenvalue Solver on a Photonic Quantum Processor. *Nat. Commun.* **2014**, *5*, 4213.
- (3) Grimsley, H. R.; Economou, S. E.; Barnes, E.; Mayhall, N. J. An adaptive variational algorithm for exact molecular simulations on a quantum computer. *Nat. Commun.* **2019**, *10*.
- (4) McArdle, S.; Jones, T.; Endo, S.; Li, Y.; Benjamin, S. C.; Yuan, X. Variational ansatz-based quantum simulation of imaginary time evolution. *npj Quantum Inf.* **2019**, *5*, 75.

- (5) Motta, M.; Sun, C.; Tan, A. T.; O'Rourke, M. J.; Ye, E.; Minnich, A. J.; Brandao, F. G.; Chan, G. K.-L. Determining eigenstates and thermal states on a quantum computer using quantum imaginary time evolution. *Nat. Phys.* **2020**, *16*, 205.
- (6) Smart, S. E.; Mazziotti, D. A. Quantum solver of contracted eigenvalue equations for scalable molecular simulations on quantum computing devices. *Phys. Rev. Lett.* **2021**, *126*, 070504.
- (7) Kyaw, T. H.; Soley, M. B.; Allen, B.; Bergold, P.; Sun, C.; Batista, V. S.; Aspuru-Guzik, A. Boosting quantum amplitude exponentially in variational quantum algorithms. *Quantum Sci. Technol.* **2023**, *9*, 01LT01.
- (8) Whitfield, J. D.; Biamonte, J.; Aspuru-Guzik, A. Simulation of electronic structure Hamiltonians using quantum computers. *Mol. Phys.* **2011**, *109*, 735.
- (9) Seeley, J. T.; Richard, M. J.; Love, P. J. The Bravyi-Kitaev transformation for Quantum Computation of Electronic Structure. *J. Chem. Phys.* **2012**, *137*, 224109.
- (10) Dutta, R.; Cabral, D. G.; Lyu, N.; Vu, N. P.; Wang, Y.; Allen, B.; Dan, X.; Cortiñas, R. G.; Khazaei, P.; Smart, S. E., et al. Simulating Chemistry on Bosonic Quantum Devices. *arXiv preprint arXiv:2404.10214* **2024**,
- (11) Huh, J.; Guerreschi, G.; Peropadre, B.; McClean, J. R.; Aspuru-Guzik, A. Boson sampling for molecular vibronic spectra. *Nature Photon.* **2015**, *9*, 615.
- (12) Wang, C. S.; Curtis, J. C.; Lester, B. J.; Zhang, Y.; Gao, Y. Y.; Freeze, J.; Batista, V. S.; Vaccaro, P. H.; Chuang, I. L.; Frunzio, L.; Jiang, L.; Girvin, S. M.; Schoelkopf, R. J. Efficient Multiphoton Sampling of Molecular Vibronic Spectra on a Superconducting Bosonic Processor. *Phys. Rev. X* **2020**, *10*, 021060.
- (13) Wang, C. S.; Frattini, N. E.; Chapman, B. J.; Puri, S.; Girvin, S. M.; Devoret, M. H.;

- Schoelkopf, R. J. Observation of wave-packet branching through an engineered conical intersection. *Phys. Rev. X* **2023**, *13*, 011008.
- (14) Lyu, N.; Miano, A.; Tsioutsios, I.; Cortiñas, R. G.; Jung, K.; Wang, Y.; Hu, Z.; Geva, E.; Kais, S.; Batista, V. S. Mapping Molecular Hamiltonians into Hamiltonians of Modular cQED Processors. *J. Chem. Theory Comput.* **2023**, *19*, 6564.
- (15) Copetudo, A.; Fontaine, C. Y.; Valadares, F.; Gao, Y. Y. Shaping photons: Quantum information processing with bosonic cQED. *Appl. Phys. Lett.* **2024**, *124*, 080502.
- (16) Deleglise, S.; Dotsenko, I.; Sayrin, C.; Bernu, J.; Brune, M.; Raimond, J.-M.; Haroche, S. Reconstruction of non-classical cavity field states with snapshots of their decoherence. *Nature* **2008**, *455*, 510.
- (17) Hacker, B.; Welte, S.; Daiss, S.; Shaukat, A.; Ritter, S.; Li, L.; Rempe, G. Deterministic creation of entangled atom–light Schrödinger-cat states. *Nature Photon.* **2019**, *13*, 110.
- (18) Bruzewicz, C. D.; Chiaverini, J.; McConnell, R.; Sage, J. M. Trapped-ion quantum computing: Progress and challenges. *Appl. Phys. Rev.* **2019**, *6*, 021314.
- (19) Joshi, A.; Noh, K.; Gao, Y. Y. Quantum information processing with bosonic qubits in circuit QED. *Quantum Sci. Technol.* **2021**, *6*, 033001.
- (20) Blais, A.; Grimsmo, A. L.; Girvin, S. M.; Wallraff, A. Circuit quantum electrodynamics. *Rev. Mod. Phys.* **2021**, *93*, 025005.
- (21) Ring, P.; Schuck, P. *The Nuclear Many-Body Problem*; Springer-Verlag, 1980.
- (22) Garbaczewski, P. The method of Boson expansions in quantum theory. *Phys. Rep.* **1978**, *36*, 65.
- (23) Klein, A.; Marshalek, E. Boson realizations of Lie algebras with applications to nuclear physics. *Rev. Mod. Phys.* **1991**, *63*, 375.

- (24) Ginocchio, J. N.; Johnson, C. W. Fermion to boson mappings revisited. *Phys. Rep.* **1996**, *264*, 153.
- (25) Von Delft, J.; Schoeller, H. Bosonization for beginners—refermionization for experts. *Ann. Phys.* **1998**, *510*, 225.
- (26) Scuseria, G. E.; Henderson, T. M.; Bulik, I. W. Particle-particle and quasiparticle random phase approximations: Connections to coupled cluster theory. *J. Chem. Phys.* **2013**, *139*, 104113.
- (27) Liu, J. A unified theoretical framework for mapping models for the multi-state Hamiltonian. *J. Chem. Phys.* **2016**, *145*, 204105.
- (28) Montoya-Castillo, A.; Markland, T. E. On the exact continuous mapping of fermions. *Sci. Rep.* **2018**, *8*, 1.
- (29) Ohta, K. New bosonic excitation operators in many-electron wave functions. *Int. J. Quantum Chem.* **1998**, *67*, 71.
- (30) Dhar, A.; Mandal, G.; Suryanarayana, N. V. Exact operator bosonization of finite number of fermions in one space dimension. *J. High Energy Phys.* **2006**, *2006*, 118.
- (31) Qin, M.; Schäfer, T.; Andergassen, S.; Corboz, P.; Gull, E. The Hubbard model: A computational perspective. *Annu. Rev. Condens. Matter Phys.* **2022**, *13*, 275.
- (32) Szabo, A.; Ostlund, N. S. *Modern Quantum Chemistry*; Dover Publications, 1996.
- (33) Helgaker, T.; Jørgensen, P.; Olsen, J. *Molecular Electronic Structure Theory*; John Wiley and Sons, 2000.
- (34) Jordan, P. Der Zusammenhang der symmetrischen und linearen Gruppen und das Mehrkörperproblem. *Zeitschrift für Physik* **1935**, *94*, 531.
- (35) Nakatsuji, H. Structure of the exact wave function. *J. Chem. Phys.* **2000**, *113*, 2949.

- (36) Fukutome, H. The Group Theoretical Structure of Fermion Many-Body Systems Arising from the Canonical Anticommutation Relation. I. *Prog. Theor. Phys.* **1981**, *56*, 809.
- (37) Suryanarayana, N. V. Half-BPS giants, free fermions and microstates of superstars. *J. High Energy Phys.* **2006**, *2006*, 82.
- (38) Wang, Y.; Hu, Z.; Sanders, B. C.; Kais, S. Qudits and high-dimensional quantum computing. *Front. Phys.* **2020**, *8*, 589504.
- (39) Hehre, W. J.; Stewart, R. F.; Pople, J. A. Self-consistent molecular-orbital methods. I Use of Gaussian expansions of Slater-type atomic orbitals. *J. Chem. Phys.* **1969**, *51*, 2657.
- (40) Divochiy, A.; Marsili, F.; Bitauld, D.; Gaggero, A.; Leoni, R.; Mattioli, F.; Korneev, A.; Seleznev, V.; Kaurova, N.; Minaeva, O., et al. Superconducting nanowire photon-number-resolving detector at telecommunication wavelengths. *Nature Photon.* **2008**, *2*, 302.
- (41) Kardynał, B.; Yuan, Z.; Shields, A. An avalanche-photodiode-based photon-number-resolving detector. *Nature Photon.* **2008**, *2*, 425.
- (42) Xu, L.; Zhou, M.; Tao, R.; Zhong, Z.; Wang, B.; Cao, Z.; Xia, H.; Wang, Q.; Zhan, H.; Zhang, A.; Yu, S.; Xu, N.; Dong, Y.; Ren, C.; Zhang, L. Resource-Efficient Direct Characterization of General Density Matrix. *Phys. Rev. Lett.* **2024**, *132*, 030201.
- (43) Hofheinz, M.; Weig, E.; Ansmann, M.; Bialczak, R. C.; Lucero, E.; Neeley, M.; O'connell, A.; Wang, H.; Martinis, J. M.; Cleland, A. Generation of Fock states in a superconducting quantum circuit. *Nature* **2008**, *454*, 310.
- (44) Gao, Y. Y.; Lester, B. J.; Zhang, Y.; Wang, C.; Rosenblum, S.; Frunzio, L.; Jiang, L.; Girvin, S. M.; Schoelkopf, R. J. Programmable Interference between Two Microwave Quantum Memories. *Phys. Rev. X* **2018**, *8*, 021073.

- (45) Zhang, Y.; Lester, B. J.; Gao, Y. Y.; Jiang, L.; Schoelkopf, R. J.; Girvin, S. M. Engineering bilinear mode coupling in circuit QED: Theory and experiment. *Phys. Rev. A* **2019**, *99*, 012314.
- (46) Gertler, J. M.; van Geldern, S.; Shirol, S.; Jiang, L.; Wang, C. Experimental Realization and Characterization of Stabilized Pair-Coherent States. *PRX Quantum* **2023**, *4*, 020319.
- (47) Shang, Z.-X.; Zhong, H.-S.; Zhang, Y.-K.; Yu, C.-C.; Yuan, X.; Lu, C.-Y.; Pan, J.-W.; Chen, M.-C. Boson sampling enhanced quantum chemistry. *arXiv preprint arXiv:2403.16698* **2024**,
- (48) You, X.; Lu, Y.; Kim, T.; Kurkcuoglu, D. M.; Zhu, S.; van Zanten, D.; Roy, T.; Lu, Y.; Chakram, S.; Grassellino, A.; Romanenko, A.; Koch, J.; Zorzetti, S. Crosstalk-Robust Quantum Control in Multimode Bosonic Systems. *arXiv preprint arXiv:2403.00275* **2024**,
- (49) Lloyd, S.; Braunstein, S. L. Quantum Computation over Continuous Variables. *Phys. Rev. Lett.* **1999**, *82*, 1784.
- (50) Braunstein, S. L.; van Loock, P. Quantum information with continuous variables. *Rev. Mod. Phys.* **2005**, *77*, 513.
- (51) Krastanov, S.; Albert, V. V.; Shen, C.; Zou, C.-L.; Heeres, R. W.; Vlastakis, B.; Schoelkopf, R. J.; Jiang, L. Universal control of an oscillator with dispersive coupling to a qubit. *Phys. Rev. A* **2015**, *92*, 040303.
- (52) Heeres, R. W.; Vlastakis, B.; Holland, E.; Krastanov, S.; Albert, V. V.; Frunzio, L.; Jiang, L.; Schoelkopf, R. J. Cavity State Manipulation Using Photon-Number Selective Phase Gates. *Phys. Rev. Lett.* **2015**, *115*, 137002.

- (53) Fösel, T.; Krastanov, S.; Marquardt, F.; Jiang, L. Efficient cavity control with SNAP gates. *arXiv preprint arXiv:2004.14256* **2020**,
- (54) Eickbusch, A.; Sivak, V.; Ding, A. Z.; Elder, S. S.; Jha, S. R.; Venkatraman, J.; Royer, B.; Girvin, S. M.; Schoelkopf, R. J.; Devoret, M. H. Fast universal control of an oscillator with weak dispersive coupling to a qubit. *Nat. Phys.* **2022**, *18*, 1464.
- (55) Chakram, S.; He, K.; Dixit, A. V.; Oriani, A. E.; Naik, R. K.; Leung, N.; Kwon, H.; Ma, W.-L.; Jiang, L.; Schuster, D. I. Multimode photon blockade. *Nat. Phys.* **2022**, *18*, 879.
- (56) Diring, A. A.; Blumenthal, E.; Grinberg, A.; Jiang, L.; Hacoen-Gourgy, S. Conditional-not Displacement: Fast Multioscillator Control with a Single Qubit. *Phys. Rev. X* **2024**, *14*, 011055.
- (57) Vlastakis, B.; Kirchmair, G.; Leghtas, Z.; Nigg, S. E.; Frunzio, L.; Girvin, S. M.; Mirrahimi, M.; Devoret, M. H.; Schoelkopf, R. J. Deterministically encoding quantum information using 100-photon Schrödinger cat states. *Science* **2013**, *342*, 607.
- (58) Lanyon, B. P.; Whitfield, J. D.; Gillett, G. G.; Goggin, M. E.; Almeida, M. P.; Kassal, I.; Biamonte, J. D.; Mohseni, M.; Powell, B. J.; Barbieri, M., et al. Towards quantum chemistry on a quantum computer. *Nature Chem.* **2010**, *2*, 106.
- (59) Arrazola, J. M.; Jahangiri, S.; Delgado, A.; Ceroni, J.; Izaac, J.; Száva, A.; Azad, U.; Lang, R. A.; Niu, Z.; Di Matteo, O., et al. Differentiable quantum computational chemistry with PennyLane. *arXiv preprint arXiv:2111.09967* **2021**,
- (60) Goss, N.; Morvan, A.; Marinelli, B.; Mitchell, B. K.; Nguyen, L. B.; Naik, R. K.; Chen, L.; Jünger, C.; Kreikebaum, J. M.; Santiago, D. I.; Wallman, J. J.; Siddiqi, I. High-fidelity qutrit entangling gates for superconducting circuits. *Nat. Commun.* **2022**, *13*, 7481.

- (61) Ryabinkin, I. G.; Yen, T.-C.; Genin, S. N.; Izmaylov, A. F. Qubit Coupled Cluster Method: A Systematic Approach to Quantum Chemistry on a Quantum Computer. *J. Chem. Theory Comput.* **2018**, *14*, 6317.
- (62) Werner, H.-J.; Manby, F. R.; Knowles, P. J. Fast linear scaling second-order Møller-Plesset perturbation theory (MP2) using local and density fitting approximations. *J. Chem. Phys.* **2003**, *118*, 8149.
- (63) Hohenstein, E. G.; Parrish, R. M.; Martínez, T. J. Tensor hypercontraction density fitting. I. Quartic scaling second- and third-order Møller-Plesset perturbation theory. *J. Chem. Phys.* **2012**, *137*, 044103.